Bioactive Materials 24 (2023) 37–53

Contents lists available at ScienceDirect

Bioactive Materials

journal homepage: www.keaipublishing.com/en/journals/bioactive-materials

Synergistically targeting synovium STING pathway for rheumatoid arthritis treatment

Haotian Shen [a,1], Lulu Jin [b,1], Qiangqiang Zheng [a,c,1], Ziqiang Ye [b], Linxiang Cheng [a], Yuxu Wu [a,d], Honghao Wu [a], Tae Gyong Jon [a], Wenduo Liu [a], Zongyou Pan [a,c,***], Zhengwei Mao [b,*], Yue Wang [a,**]

[a] Department of Orthopedic Surgery, The First Affiliated Hospital, Zhejiang University School of Medicine, Hangzhou, 310003, China
[b] MOE Key Laboratory of Macromolecular Synthesis and Functionalization, Department of Polymer Science and Engineering, Zhejiang University, Hangzhou, 310027, China
[c] Dr. Li Dak Sum & Yip Yio Chin Center for Stem Cells and Regenerative Medicine, Zhejiang University School of Medicine, Hangzhou, 310000, China
[d] International Institutes of Medicine, The Fourth Affiliated Hospital, Zhejiang University School of Medicine, N1 Shangchen Road, Yiwu, Zhejiang, 322000, China

ARTICLE INFO

Keywords:
Mesoporous nanoparticles
STING
Inflammation
Drug delivery
Rheumatoid arthritis

ABSTRACT

Rheumatoid arthritis (RA) is a common autoimmune disease leading to pain, disability, and even death. Although studies have revealed that aberrant activation of STING was implicated in various autoimmune diseases, the role of STING in RA remains unclear. In the current study, we demonstrated that STING activation was pivotal in RA pathogenesis. As the accumulation of dsDNA, a specific stimulus for STING, is a feature of RA, we developed a spherical polyethyleneimine-coated mesoporous polydopamine nanoparticles loaded with STING antagonist C-176 (PEI-PDA@C-176 NPs) for treating RA. The fabricated NPs with biocompatibility had high DNA adsorption ability and could effectively inhibit the STING pathway and inflammation in macrophages. Intra-articular administration of PEI-PDA@C-176 NPs could effectively reduce joint damage in mice models of dsDNA-induced arthritis and collagen-induced arthritis by inhibiting STING pathway. We concluded that materials with synergistic effects of STING inhibition might be an efficacious strategy to treat RA.

1. Introduction

Rheumatoid arthritis (RA) is a common autoimmune disease, affecting approximately 17.5 million people globally in 2017 [1]. As a chronic inflammatory disease leading to pain, disability and eventually death, RA reduces the life expectancy by approximately five years for each patient, adding a heavy burden on families and societies [2]. Current treatments for RA, such as nonsteroidal anti-inflammatory drugs and glucocorticoids, mainly focus on pain control and joint function maintenance [3,4]. However, these treatments, have relatively low response rates [5] and high odds of adverse effects [6]. Although RA pathogenesis has not been fully understood, one of the major mechanisms is the aberrant immune response, which attacks various articular tissues, resulting in persistent synovitis and progressive destruction of cartilage and subchondral bone [7]. An important approach to improve clinical treatment of RA is to identify new therapeutic targets in the unbalanced immune response and develop novel interventional strategies [8,9].

The Stimulator of interferon genes (STING) has attracted considerable interest in various inflammatory diseases [10–12]. After cyclic GMP-AMP synthase (cGAS) senses cell-free DNA (cfDNA), STING recruits kinases, including tank-binding kinase 1 (TBK1) and its target protein interferon regulatory factor 3 (IRF3), and facilitates their phosphorylation (pTBK1 and pIRF3) [13]. Dysregulation of the STING

Peer review under responsibility of KeAi Communications Co., Ltd.
* Corresponding author. MOE Key Laboratory of Macromolecular Synthesis and Functionalization, Department of Polymer Science and Engineering, Zhejiang University, Hangzhou, 310027, China.
** Corresponding author. Department of Orthopedic Surgery, The First Affiliated Hospital, Zhejiang University School of Medicine, Hangzhou, 310003, China.
*** Corresponding author. Dr. Li Dak Sum & Yip Yio Chin Center for Stem Cells and Regenerative Medicine, Zhejiang University School of Medicine, Hangzhou, 310003, China.
E-mail addresses: panzongyou@zju.edu.cn (Z. Pan), zwmao@zju.edu.cn (Z. Mao), wangyuespine@zju.edu.cn (Y. Wang).
[1] These authors contributed equally to this work.

https://doi.org/10.1016/j.bioactmat.2022.12.001
Received 1 July 2022; Received in revised form 23 October 2022; Accepted 1 December 2022

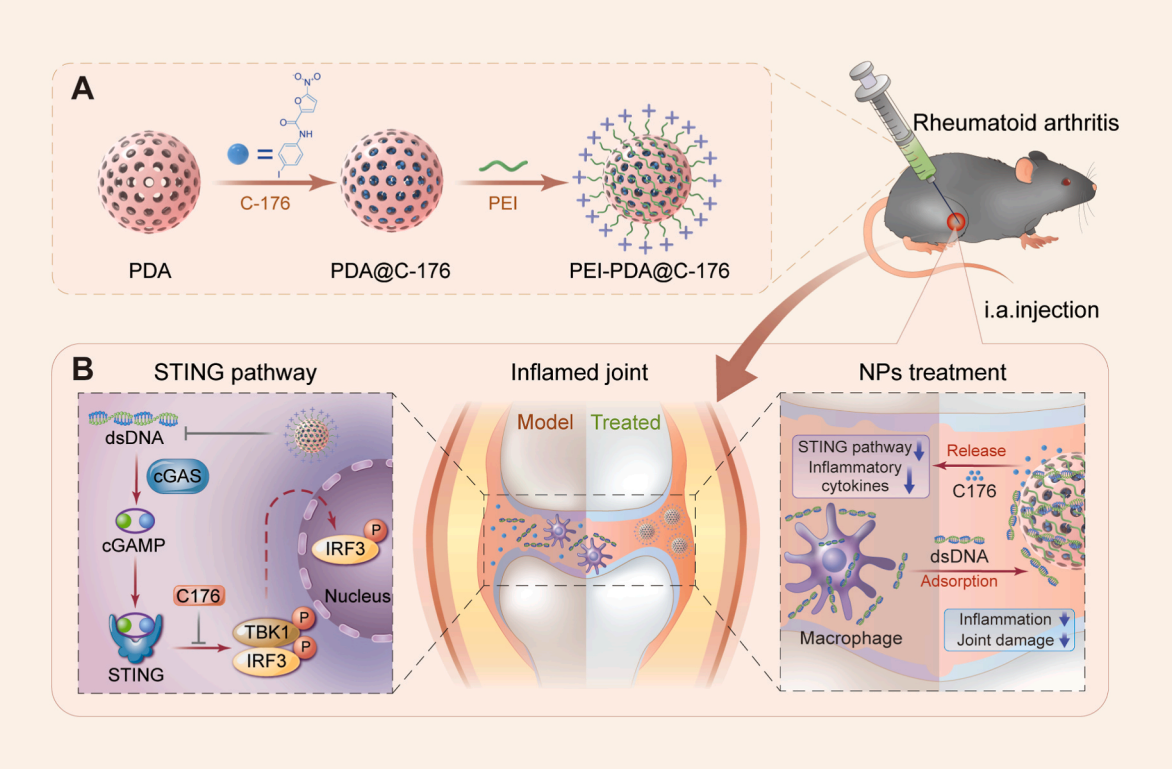

Scheme 1. Schematic illustration of PEI-PDA@C-176 NPs as a therapeutic for RA via inhibiting the STING pathway. (**A**) The PDA NPs were loaded with STING antagonist C-176, and the surface of PDA@C176 NPs was further decorated with PEI to obtain a high DNA-binding affinity. (**B**) Mechanisms of the PEI-PDA@C-176 NPs in treating RA. The compound can adsorb the STING stimulus dsDNA and inhibit STING palmitoylation simultaneously. As a result, PEI-PDA@C-176 NPs showed a marked effect on alleviating RA inflammation and pathogenesis. i. a., intra-articular. dsDNA, double-stranded DNA.

pathway can upregulate various inflammation-related genes [14] and disrupt cellular homeostasis by promoting aberrant innate immune response [15–17]. Given the critical role of STING in inflammatory diseases, STING antagonists have attracted significant attention. Recent studies have reported that C-176, a small-molecule drug, can effectively block the activation of STING [18] and thus, attenuate inflammation in inflammatory diseases such as acute lung injury [19], hypercholesterolemia [20], and pulmonary fibrosis [21]. Although arthritis is a common inflammatory disease, the role of STING signaling in RA is not fully elucidated. While one study has revealed that STING activation promoted the progression of osteoarthritis via the nuclear factor kappa B (NF-κB) pathway [22], another study has reported that STING was a negative regulator of B cells in RA [23]. Given the aberrant activation of STING in various inflammatory diseases, particularly autoimmune diseases [24], the role of STING in RA deserves further investigation and inhibition of STING might serve as an alternative treatment for RA.

Specifically modified biomaterials can capture proinflammatory factors that otherwise may initiate multiple pathological signaling [25,26]. For example, modified cationic polymers can adsorb DNA and prevent DNA-induced immune responses in macrophages [27,28]. Double-stranded DNA (dsDNA), which is released from damaged or dead cells, is one of the biological features in RA pathology [29]. Interestingly, dsDNA is also a specific stimulus for STING [30]. Hence, scavenging dsDNA with cationic nanoparticles (NPs) may reduce STING activation and alleviate inflammation. Yet, cationic NPs of high concentration have considerable cytotoxicity and, thus, might not be suitable for medical use [31]. NPs with synergistic functions, which can improve the efficiency of a drug in a relatively low concentration, might be a solution for this challenge [32]. Besides, NPs also have multiple advantages in drug delivery, including targeted delivery, sustained release, improved bioavailability, and reduced side effects [33–35]. Therefore, we hypothesized that optimized cationic NPs might scavenge dsDNA and synergistically inhibit STING pathway in the presence of STING antagonists.

In this study, we first examined dsDNA accumulation and STING activation in human and mouse RA synovial tissues, and then investigated the functional consequences of STING on RA with genetic ablation of *STING* in mice (*Sting1*$^{+/-}$ mice). Furthermore, mesoporous polydopamine (PDA) NPs were developed for local delivery of C-176 and the surface of NPs was decorated with optimized cationic polyethyleneimine (PEI) to obtain a high DNA-binding affinity (Scheme 1). The strength of these PEI-PDA@C-176 NPs was the synergetic inhibition of STING signaling and dsDNA-induced immune responses in macrophages, which allowed for a reduced dose of drugs while acquiring satisfactory effects. The efficacy of PEI-PDA@C-176 NPs in treating RA was further tested in two arthritis models and *Sting1*$^{+/-}$ mice.

2. Materials and methods

2.1. Study design

The objectives of this study were to investigate the role of the STING pathway in RA pathogenies and develop materials for RA treatment. Thus, we first examined dsDNA accumulation and STING activation in human and mouse RA synovial tissues. We investigated the contribution of the STING pathway to RA pathogenesis using *STING* knockout mice. Upon these findings and the fact that dsDNA is a specific stimulus for STING, we developed a PDA-based nanoparticle to simultaneously capture dsDNA and deliver STING antagonist C-176. The function of PEI-PDA@C-176 NPs in the inhibition of the STING pathway and inflammation was comprehensively studied *in vitro*. Then, we analyzed the function of PEI-PDA@C-176 NPs in treating RA in two mice models of RA, including dsDNA-induced arthritis and CIA. Furthermore, we examined how PEI-PDA@C-176 NPs alleviated inflammation through

the STING pathway in *STING* knockout mice. For each experiment, sample sizes for independent experiments are indicated in the figure legend. All studies involving human samples and animals were approved by the ethical review board at the author's institute. Written consent was obtained from all patients before the operation.

2.2. Chemicals

Dopamine hydrochloride and tris(hydroxymethyl)aminomethane were obtained from Sinopharm Chemical Reagent, China. Pluronic® F127 (Mw ~13 kD), polyethyleneimine (PEI, Mw ~10 kD), deoxyribonucleic acid from herring sperm (D7290), 10-carboxymethyl-9-acridanone (CMA) and 1,3,5-trimethylbenzene (TMB) were purchased from Sigma-Aldrich, USA. C-176 was purchased from MCE, USA. CpG 1826 and Cy5-CpG 1826 were obtained from Sangon Biotech, China. All other chemicals were of analytical grade and used as received, if not described otherwise. Water was purified by the Milli-Q system prior to use in the experiments.

2.3. Assessment of human synovium samples

All experiments related to human samples were approved by the ethical review board at the author's institute (ethic code: ZDYY-20210136B). Each patient understood the study protocol and signed written consent. Synovium specimens were obtained from three RA patients who underwent total knee arthroplasty. Control synovium specimens were obtained from three patients who underwent arthroscopic meniscus repair surgery and had no synovitis and cartilage injury on arthroscopy. Synovial tissues were used for western blotting and histological analysis to study the activation of the STING pathway in RA.

2.4. Animals

Male DBA/1 mice (6 weeks), C57/B6 mice (6 weeks), and BALB/c mice (6 weeks) were purchased from the Animal Center at the author's institute. *Sting1*$^{+/-}$ mice were purchased from GemPharmatech, China. In the animal facility at the author's institute, mice were bred, housed and used in a specific pathogen-free environment. All animal studies were performed with the approval of the ethical review board at the author's institute (ethic code: ZDYY-2021-917).

2.5. CIA model in WT and *Sting1*$^{+/-}$ mice

Before modeling, *Sting1*$^{+/-}$ and wild-type (WT) mice received tamoxifen (Sigma-Aldrich, USA) via intraperitoneal injection (100 μg/g per day) for five days. Then, 8 *Sting1*$^{+/-}$ mice (male, 8-week-old) and 8 WT C57/B6 mice (male, 8-week-old) were used to establish the CIA model [36,37]. First, bovine type II collagen (2 mg/mL, Chondrex, USA) dissolved in acetic acid was mixed with an equal amount of Complete Freund's adjuvant (CFA, Chondrex, USA) using a handheld homogenizer in an ice bath for 30 min. On days 0 and 7, 0.1 mL emulsion was subcutaneously injected via the tail. Mice were sacrificed 60 days after the modeling. Both ankle joints were harvested and dissected for histological analysis.

2.6. Synthesis of PDA NPs

The PDA NPs were prepared according to a previous report [38]. Briefly, 0.36 g pluronic F127 and 0.36 g TMB were dissolved in 125 mL H_2O/ethanol mixture solution (v:v = 1:1) and stirred for 30 min. 90 mg tris(hydroxymethyl)aminomethane and 60 mg dopamine hydrochloride were dissolved in 10 mL water and then introduced to the mixture. After the reaction at room temperature for 24 h, the particles were collected via centrifugation. In the presence of sonication, the polymer micelle templates were washed off using tetrahydrofuran for 30 min. Washing was repeated for three times.

C-176 was encapsulated into PDA NPs by deposition. Different amount of C-176 was incubated with PDA NPs (20 mg/mL) in THF/water solution at room temperature for 12 h. PDA@C-176 NPs were collected via centrifugation and water-washed to remove unloaded C-176. The surface of PDA NPs was then modified with PEI via physical adsorption. 20 mg PDA@C-176 NPs were incubated in 1 mL PEI solution (1 mg/mL) and mixed under vortex for 15 min. After three cycles of centrifugation and washing, PEI-PDA@C-176 NPs were obtained.

Using UV–visible spectroscopy (UV2550, Shimadzu, Japan), the loading amount of C-176 in PDA NPs was quantified as the difference of C-176 concentration in the feeding solution before and after PDA NP treatment.

PDA NPs (20 mg/mL) were also covalently labeled with fluorescein isothiocyanate (FITC, Sigma, 0.2 mg/mL) or Cy5 succinimidyl ester (Cy5-NHS, GLPBIO, 0.2 mg/mL) to obtain FITC-PDA or Cy5-PDA NPs, respectively. To covalently label PDA NPs with FITC, PDA NPs (20 mg/mL) were mixed with fluorescein (0.2 mg/mL) and shaken overnight. The obtained FITC-labeled PDA NPs were then centrifuged and washed three times to remove free fluorescein. The obtained FITC-PDA and Cy5-PDA NPs were trackable under fluorescent microscopy.

2.7. Characterization of PDA NPs

A dynamical laser scattering assay was performed with a nano analyzer (Malvern, UK) to characterize the hydrodynamic diameter and surface zeta potential of PDA NPs. Morphology of NPs was observed with a transmission electron microscope (HT7700, Hitachi, Japan).

PDA@C-176 NPs were suspended in phosphate-buffered saline (PBS) containing 1% Tween-80 at 37 °C to test sustained release of C-176. The suspension was centrifuged at 10000×*g* for 30 min at pre-designed time points. Then, 2 mL supernatant was taken out and 2 mL fresh PBS was added. The concentration of C-176 was then determined using high-performance liquid chromatography (HPLC) with a 280-nm detector.

DNA binding ability of PDA NPs was also tested. Various concentrations of DNA solutions (5 μg/mL - 30 μg/mL) were incubated with different PDA NPs (1 mg/mL) (N/P 200 - N/P 33) for 12 h under vortex at 37 °C. In addition, 20 μg/mL DNA solution was incubated with different PDA NPs (1 mg/mL) (N/P 50) for a predetermined period. After centrifugation, the DNA concentration in the supernatant was quantified using a Picogreen assay (Thermo Fisher).

2.8. Gel retardation assay

PDA NPs and DNA (N/P)were dissolved in PBS prior to experiments. Then, 10 mL of PDA (1 mg/mL) NP solution were mixed with 1 mL DNA solution (0.2 mg/mL) (N/P 50) under vortex for 15 s and further incubated for 30 min. The retardation assay was performed with 100 μl of complex suspensions running on a 1% agarose gel at 100 V for 40 min at 37 °C.

2.9. Biodistribution of PEI-PDA@C-176 NPs

Three CIA model mice (male, 12-week-old) and 3C57/B6 mice (male, 12-week-old) were used to study the biodistribution of materials. 10 μL Cy5-labeled PEI-PDA NPs and PDA NPs were injected into the knee joint, respectively. The biodistribution of the materials was monitored on days 1, 3, 5, and 7.

2.10. Toxicity evaluation

A live/dead cell viability assay was performed after the incubation of RAW264.7 cells in 1 mg/mL PDA NPs for 24 h to evaluate the cytotoxicity of PDA NPs. Then, the proportion of live cells was calculated from images obtained with a confocal fluorescence microscope (IX83-FV3000, Olympus, Japan). Besides, the Cell Counting Kit-8 (CCK8, Beyotime) was used according to the instructions. RAW264.7 cells were

treated with 1 mg/mL PDA NPs for 24 h and then cultured in CCK8 staining solution for 2 h. The optical density at 450 nm was measured to determine the relative viable cell numbers.

C57/B6 mice (male, 12-week old) were used to evaluate the biocompatibility of NPs *in vivo*. Intra-articular injection of the following drugs was performed for the knee joints at a dose of 5 μL once per week: 1 mg/mL PEI-PDA NPs, 1 mg/mL PDA@C-176 NPs, and 1 mg/mL PEI-PDA@C-176 NPs. Untreated mice were used as sham controls. The mice were weighed every 6 days and sacrificed 30 days after the first injection. Blood erythrocytes, leukocytes, and hemoglobin were measured after the mice were sacrificed. The livers, kidneys, lungs, spleens, and hearts of sacrificed mice were harvested and embedded for histological analysis.

2.11. Cell experiments

Bone marrow-derived macrophages (BMDMs) were extracted from 12-week-old male C57/B6 mice. Total bone marrow cells were plated in six-well culture plates in Dulbecco's Modified Eagle Medium (DMEM, Gibco, USA) supplemented with 10% fetal bovine serum (FBS) and macrophage colony-stimulating factor (20 ng/mL, Biolegend, USA). Non-adherent cells were removed after 24 h incubation. BMDMs were incubated with 10 nM CMA for 2 h to mimic pathological conditions and then incubated in 1 mg/mL PEI-PDA, PDA@C-176, and PEI-PDA@C-176 NPs for 8 h, respectively. The cells were then harvested for western blotting.

Human primary fibroblast-like synoviocytes (FLSs) were isolated from patients' synovial tissues through enzymatic digestion using 2 mg/mL type I collagenase (Sigma-Aldrich, USA) and 0.1 mg/mL DNase I (Roche, UK) for 4 h. The dissociated cells were cultured in DMEM complemented with 10% FBS. After 24 h incubation, non-adherent cells were removed by PBS washing. FLSs were used from passage 3 to 9, and the cell type was determined as described previously [29]. FLSs were incubated with 10 μg/mL DNA for 2 h to induce dsDNA evoked change and then incubated with 1 mg/mL PEI-PDA, PDA@C-176, and PEI-PDA@C-176 NPs for 8 h, respectively. The supernatant was collected for enzyme-linked immunosorbent assay ELISA analysis of interferon β (IFNβ), tumor necrosis factor α (TNFα) and interleukin (IL)-6 using commercial ELISA kits (Biolegend, USA).

RAW264.7 cells were purchased from the Cell Bank of the Chinese Academy of Sciences (Shanghai, China). RAW264.7 cells were used to investigate the colocalization of dsDNA with PDA NPs and dsDNA clearance capability of PDA NPs.

2.12. Western blotting

Protein expression level in cells and synovial tissues was measured as described previously [39]. Incubation with antibodies was performed in accordance to the instructions with primary antibodies including pTBK1 (5483, CST), TBK1 (3013, CST), STING (13647s, CST), pIRF3 (29047, CST), IRF3 (ab25950, Abcam), and β-actin (A00702, GenScript), and secondary antibody (Invitrogen, USA). The bands were detected using western blot detection reagents (ThermoFisher, USA). Protein expression was semi-quantified using *ImageJ* (Ver 1.52, NIH, USA) and the expression levels of target proteins were expressed relative to *β-actin*.

2.13. Colocalization of dsDNA and PDA NPs in cells

This experiment was designed to test whether synthesized PEI-PDA NPs could intracellularly bind to dsDNA [27]. Cy5-labeled CpG 1826, which was obtained from Sangon Biotech, China, was used as representative dsDNA. RAW264.7 cells were first incubated in 1 μM Cy5-CpG for 4 h. After removing excessive CpG, FITC-labeled PDA and PEI-PDA NPs were added to the medium to reach the concentration of 1 mg/mL. After 8 h incubation, the treated cells were stained with DAPI for confocal microscopic observation (IX83-FV3000, Olympus, Japan).

2.14. dsDNA clearance capability of PEI-PDA NPs

This test was designed to investigate whether PEI-PDA NPs could clear cell-free dsDNA. RAW264.7 cells were first incubated with 1 μM dsDNA for 2 h. After removing excessive dsDNA, RAW264.7 cells were treated with 1 mg/mL PDA or PEI-PDA NPs for 12 h. The levels of dsDNA after treatments were measured using immunoblotting and confocal microscopy.

2.15. Effects of PEI-PDA@C-176 NPs in treating dsDNA-induced arthritis

Forty BALB/c mice (male, 12-week old) were randomly divided into 5 groups (8 mice/group): (1) sham; (2) arthritis model treated with PBS; (3) arthritis model treated with PEI-PDA NPs; (4) arthritis model treated with PDA@C-176 NPs; and (5) arthritis model treated with PEI-PDA@C-176 NPs. For mice in the model groups, 5 μL saline containing 6 μg dsDNA was injected into the right ankle joint to induce acute arthritis [27]. Immediately after the modeling, treatments with PBS, 1 mg/mL PEI-PDA, PDA@C-176, and PEI-PDA@C-176 NPs at a dose of 10 μL were injected into the right ankle joint, respectively. The treatment was performed daily till day 7. Mice in the sham group received a dsDNA-free saline injection for 7 days. The diameter of the right ankle joint was measured daily with a caliper (Guanglu, China). Mice were sacrificed on day 8 and the ankle joints were harvested for micro-computed tomography (μCT) and then embedded for histological analysis.

2.16. Effects of PEI-PDA@C-176 NPs in treating CIA

Forty DBA/1 mice (male, 12-week old) were used to study the therapeutic effects of PEI-PDA@C-176 NPs in treating CIA. Eight served as sham mice and received weekly intra-articular injections of dsDNA-free saline into the left knee. CIA model was established for 32 mice, as mentioned previously. After the onset of arthritis, which typically occurred on day 28, the arthritic mice were randomly divided into 4 groups (8 mice/group) and received the following intra-articular treatments for 32 days (once per week for 5 weeks): (1) PBS, (2) PEI-PDA NPs, (3) PDA@C-176 NPs, and (4) PEI-PDA@C-176 NPs. 10 μL PBS containing various types of PDA NPs (1 mg/mL) was given by intra-articular injection into the left knee joint. Each mouse received 5 intra-articular injections. After the sacrifice, the swelling of the knee joints was evaluated, as reported above. The knee joints were harvested for μCT study and then embedded for histological analysis.

The above experiments were repeated in 40 *Sting1*$^{+/-}$ mice (male, 12-week old) to study the underlying mechanism. The *Sting1*$^{+/-}$ mice received tamoxifen administration for 5 days before the modeling.

2.17. Clinical score of arthritis

Using a 5-point scale, two investigators who were blinded to the group allocation independently assessed the clinical score of arthritis [36]. The joint was rated as 0 if there was no sign of erythema or swelling; 1 if the joint had any erythema or mild swelling; 2 if erythema and mild swelling extended from the ankle to the tarsus; 3 if erythema and moderate swelling extended from the ankle joint to the metatarsal joint; 4 if the joint had erythema and severe swelling including ankles, paws, and stiffness of fingers or limbs. Clinical scores for 2 forelimbs and 2 hindlimbs were summed up for a mouse to have an overall arthritis severity score, with a higher score indicating more severe arthritis. Clinical scores of arthritis were averaged between two investigators for analysis.

2.18. Histological analysis

The dissected tissues were fixed in 4% formaldehyde for 48 h and then decalcified in 10% ethylene-diamine tetra acetic acid (EDTA)

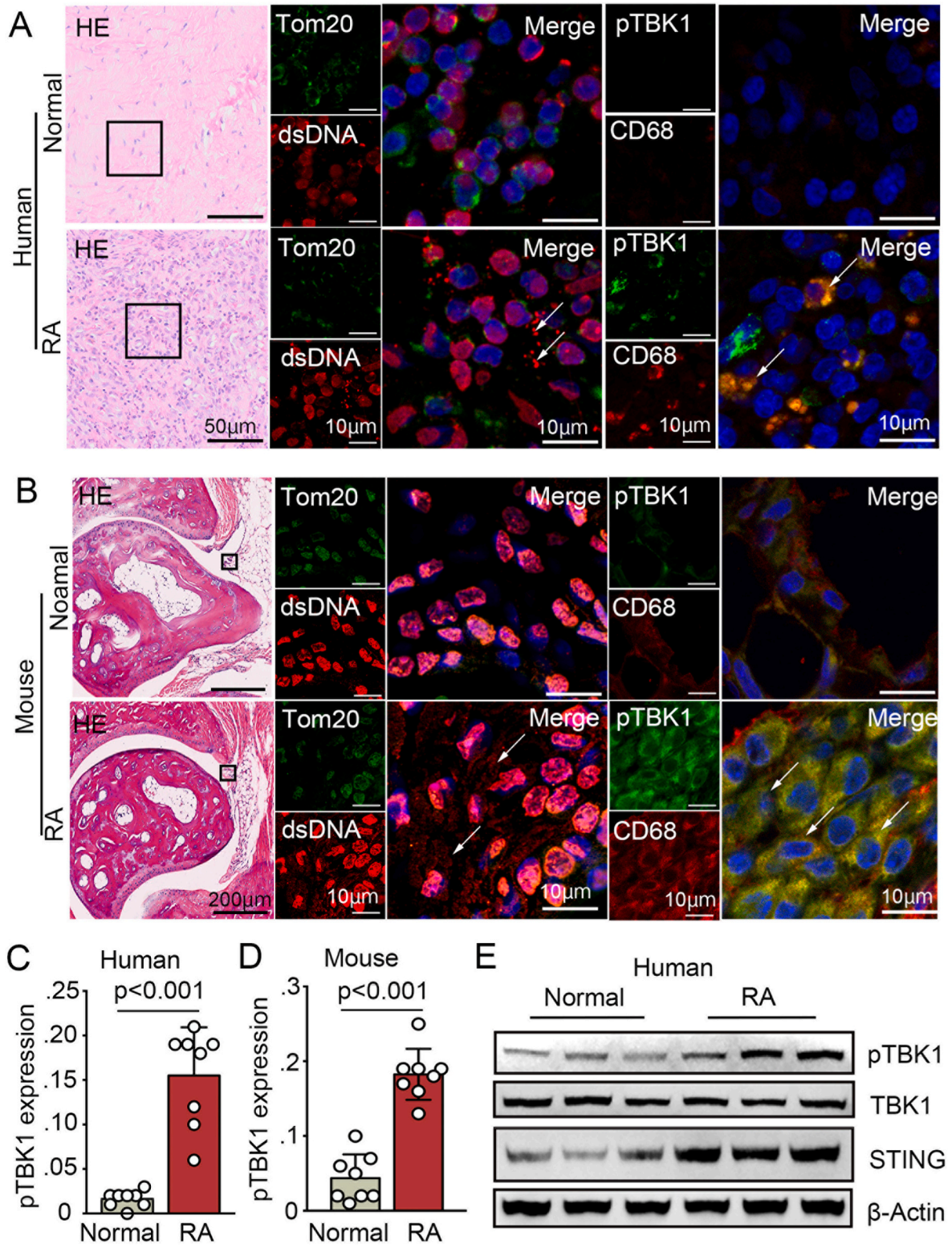

Fig. 1. dsDNA and STING signaling in the synovium from RA patients and CIA model mice. Representative images of HE staining, Tommo20/dsDNA coimmunostaining, and pTBK1/CD68 coimmunostaining of the synovium of RA patients (**A**, knee, n = 3), CIA model mice (**B**, ankle, n = 3), and corresponding normal controls. Coimmunostaining of Tommo20 and dsDNA displayed cell-free dsDNA (red) which were outside of the nucleus (blue) and mitochondria (green), as highlighted with white arrows. Coimmunostaining of pTBK1 and CD68 demonstrated increased pTBK1 expression (green) in CD68-positive macrophage (red), as indicated with white arrows. In both human (**C**) and mouse (**D**) synovium, quantitative analysis demonstrated that pTBK1 was highly expressed in RA synovium (n = 8 regions). (**E**) Immunoblotting of relative pTBK1, TBK1, STING and β-Actin expression levels in RA and normal human synovium (n = 3). Scale bars: 50 μm or 200 μm for HE staining and 10 μm for immunostaining.

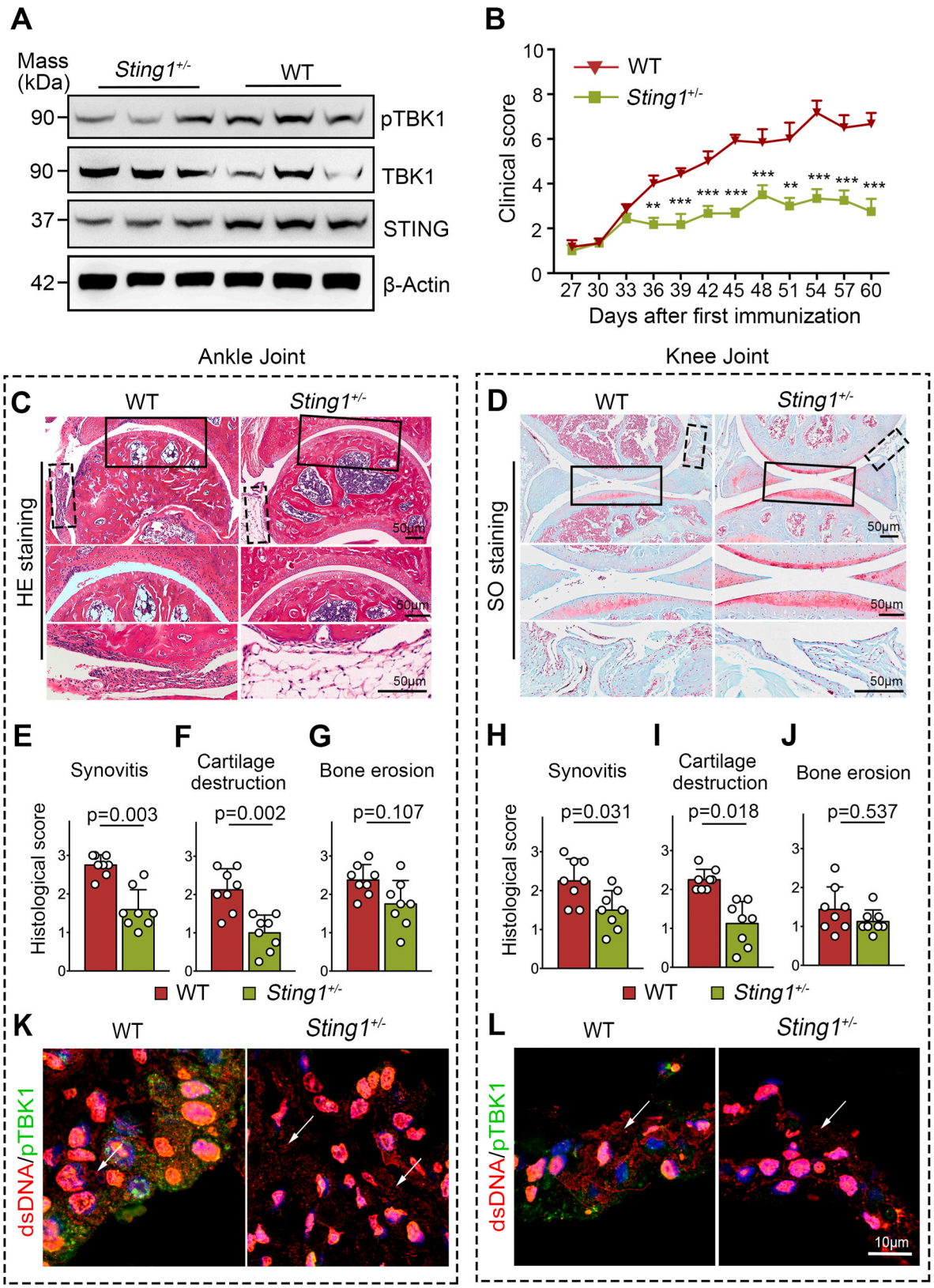

Fig. 2. Genetic deletion of *STING* ameliorated RA pathologies. (**A**) Representative immunoblotting of pTBK1, TBK1, and STING in synovium derived from WT and *Sting1*$^{+/-}$ mice (n = 3). (**B**) Clinical scores of arthritis were evaluated every 3 days (n = 8 mice per group). (**C**) HE staining of ankle joints from the CIA modeled *Sting1*$^{+/-}$ and WT mice. (**D**) Representative safranin O staining of the knee joint from CIA modeled *Sting1*$^{+/-}$ mice and WT mice. Histological score for (**E**) synovitis, (**F**) cartilage destruction, and (**G**) bone erosion graded from the ankle joints of CIA modeled *Sting1*$^{+/-}$ mice and WT mice. Histological score for (**H**) synovitis, (**I**) cartilage destruction and (**J**) bone erosion of the knee joint revealed that genetic deletion of *STING* significantly alleviated pathological changes in CIA model mice. Representative immunofluorescent staining of pTBK1 (green) and dsDNA (red) in (**K**) ankle and (**L**) knee joints from CIA modeled *Sting1*$^{+/-}$and WT mice. **P < 0.01 and ***P < 0.001. Scale bars: 50 μm (**C**) and 10 μm (**K**), respectively.

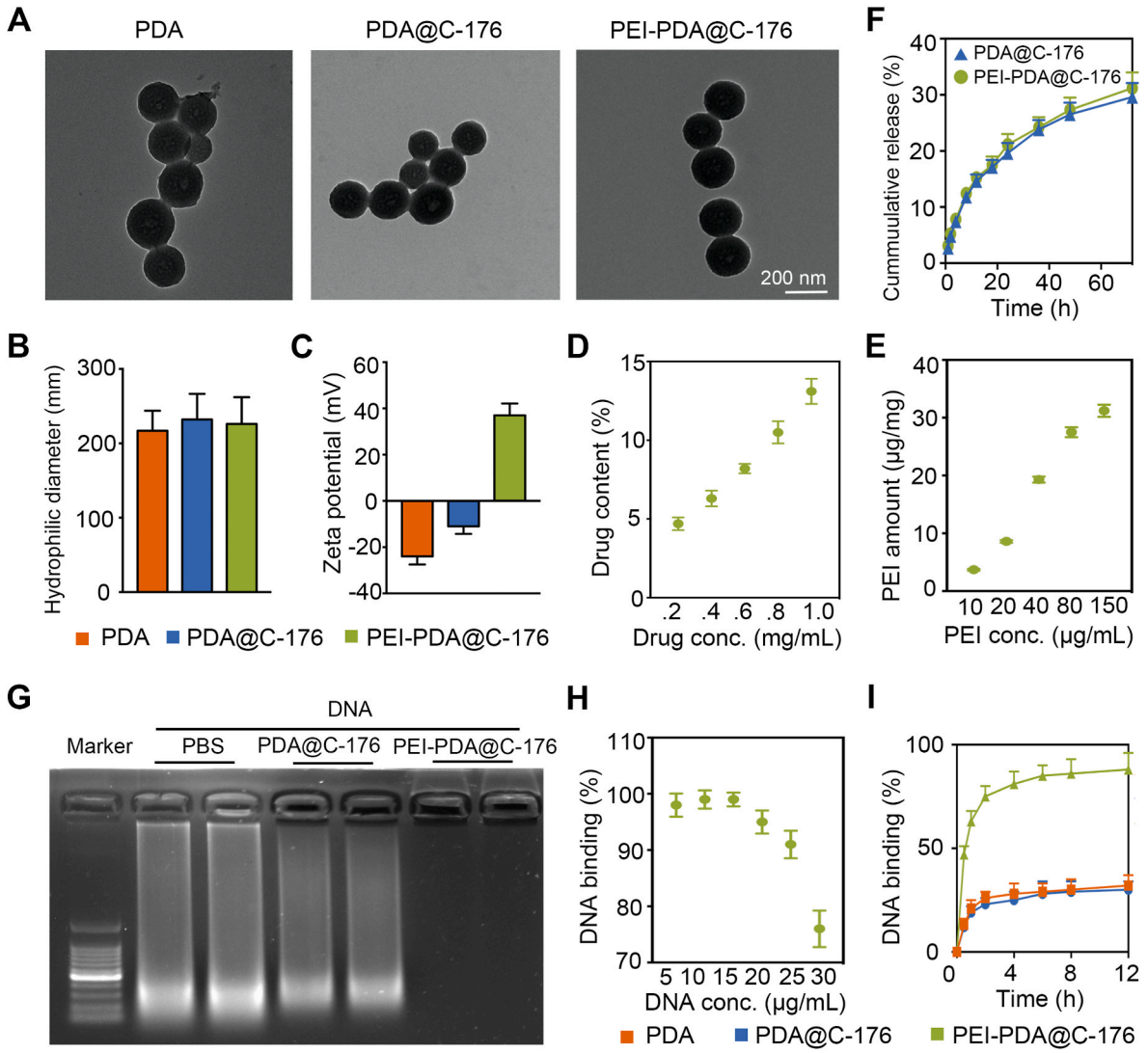

Fig. 3. Characterization of PEI-PDA@C-176 NPs. (**A**) TEM images of PDA, PDA@C-176, and PEI-PDA@C-176 NPs. (**B**) Hydrodynamic diameters and (**C**) surface zeta potentials of PDA, PDA@C-176 and PEI-PDA@C-176 NPs. (**D**) C-176 loading content in the PDA@C-176 NPs as a function of C-176 feeding concentration. (**E**) PEI amount decorated on the PEI-PDA@C-176 NPs as a function of PEI feeding concentration. (**F**) Cumulative release of C-176 from PDA@C-176 and PEI-PDA@C-176 NPs. (**G**) Agarose gel electrophoresis of free DNA, DNA + PDA@C-176, and DNA + PEI-PDA@C-176, using 1% agarose at 37 °C. DNA binding percentages of (**H**) PEI-PDA@C-176 NPs as a function of DNA concentration and (**I**) PDA based nanoparticles as a function of incubation time. conc., concentration.

solution for 30 days. Specimens were embedded, cut into 7-μm paraffin slices, and stained with hematoxylin and eosin (HE) and safranin O (SO), respectively [39]. Histological images were taken under a microscope (VS200, Olympus, Japan). Using a 4-point scale, synovitis, cartilage damage and bone erosion were separately assessed, with 0 indicating healthy and intact tissue and 3 indicating severe arthritis [40]. Histological scores were conducted by 4 independent investigators blinded to the group allocation and then averaged for analysis.

2.19. Immunohistochemistry (IHC) staining and immunofluorescence (IF) staining

IHC staining and IF staining were performed using standard procedures [39]. For immunostaining, slices were covered in 0.01 M sodium citrate buffer at 65 °C for 10 h for antigen recovery, subjected to 0.5% Triton-X 100 for 20 min to break the cell membranes, and then incubated with 10% FBS for 1 h to block non-specific binding sites. Incubation with primary antibody was performed according to the instructions, and the used primary antibodies included pTBK1 (5483, CST), CD68 (ab955, Abcam), Tommo20 (ab78547, Abcam), dsDNA (ab27156, Abcam), and Col2 (ab34712, Abcam).

For IHC staining, sections were subjected to corresponding horseradish peroxidase (HRP)-labeled secondary antibodies for 1 h. Diaminobenzidine (DAB) solution was utilized to visualize the target protein. The images were then captured with a microscope (VS200, Olympus, Japan). For IF staining, slices were incubated with fluorescent secondary antibody at 37 °C for 1 h. The slices were then stained with 4',6-diamidino-2-phenylindole (DAPI) and observed with a confocal fluorescence microscope (IX83-FV3000, Olympus, Japan). Quantitative analysis was performed with *ImageJ*. The proportion of positively stained cells was counted and averaged on at least 3 sections for analysis. Approximately 20 immunopositively stained cells were counted on each section.

2.20. μCT imaging

Prior to histological analysis, the fixed joint specimens were scanned with a μCT (Inveon Micro-CT, Siemens, German) at a resolution of 19 μm, 80-KV voltage, 500-μA current, and 300-ms exposure time. μCT images were analyzed using Materialise Mimics (V21.0, Materialise,

Belgium).

2.21. Statistical analysis

Data were expressed as mean ± standard deviation (SD). Data were analyzed using *SPSS* (Ver 23.0, IBM Corp, USA) and graphed with *GraphPad Prism* (Ver 7.0, GraphPad Software Inc, USA). The *t*-test, one-way analysis of variance (ANOVA), Tukey's multiple comparisons test, and Mann-Whitney *U* test were utilized as appropriate. The significance level was presented as *P < 0.05, **P < 0.01, and ***P < 0.001, respectively.

3. Results

3.1. Accumulation of cell-free dsDNA and activation of the STING pathway in synovium from RA patients and CIA model mice

We first examined whether STING was activated in RA synovium. As shown in Fig. 1A (HE staining), there were numerous clustered cells in the synovium of RA patients. Immunofluorescence staining revealed that the STING pathway was activated in RA synovium, as reflected by the increased fluorescence of pTBK1, which is a well-known hallmark of the STING pathway. In RA synovium, the co-localization of pTBK1 with the macrophage marker CD68 reached approximately 65% (Fig. 1A), indicating that the STING-TBK1 pathway was substantially activated in macrophages. Further, coimmunostaining of dsDNA and mitochondrial marker Tommo20 was performed to investigate the presence of cell-free dsDNA which was outside the nuclei and mitochondria. There was a massive cell-free dsDNA (red) accumulation in the RA synovium (Fig. 1A, white arrows), suggesting profound DNA damage and leakage to the intercellular space in the affected synovium. Western blot also revealed that the expression of STING and pTBK1 was significantly upregulated in RA synovium, as compared with normal synovium (Fig. 1E, Fig. S1). Overall, data suggested a potential connection between the accumulation of cell-free dsDNA and activation of the STING-pTBK1 pathway in macrophages in the RA synovium.

The CIA model mice presented hyperplasia of synovial tissues in the ankle joints (Fig. 1B, black box). Immunostaining showed that cell-free dsDNA was accumulated in the synovium in CIA model mice but was barely detectable in the synovium of sham mice (Fig. 1B). The expression level of pTBK1 in the CIA synovium was approximately 4 folds greater than that in normal mice, indicating that the STING-TBK1 pathway was significantly activated in RA mice (Fig. 1B and D). Coimmunostaining of pTBK1 and CD68 demonstrated approximately 80% of colocalization in the synovium of CIA mice, which was significantly greater than that in sham synovium (Fig. 1B). A relationship between cell-free dsDNA and STING pathway in macrophages was confirmed in the CIA model mice.

3.2. Genetic deletion of STING ameliorated RA pathogenesis

To explore the effects of the STING pathway in RA pathogenesis, we performed genetic ablation of STING using the CRISPR/Cas9 technique. As shown in Fig. 2A, expression levels of STING and pTBK1 were reduced in the synovial tissues of *Sting1*$^{+/-}$ mice, suggesting a successful *STING* knockout. The severity of arthritis was decreased in the CIA model of *Sting1*$^{+/-}$ mice, as evidenced by the substantially decreased clinical scores ($P < 0.001$, Fig. 2B).

Histological analysis of the ankle and knee joints (Fig. 2C and D) revealed that there were decreased synovial lining hyperplasia (Fig. 2E and H) and less cartilage damage (Fig. 2F and I) in the *Sting1*$^{+/-}$ mice than in the WT mice ($P < 0.05$ for all). There was also less bone damage in both ankle and knee joints in *Sting1*$^{+/-}$ mice but did not reach statistical significance (Fig. 2G and J). Immunostaining showed a significant decrease in *pTBK1* expression in *Sting1*$^{+/-}$ mice ($p < 0.001$, Fig. 2K and L) compared with that in WT mice. Still, dsDNA was presented in the joint tissues in *Sting1*$^{+/-}$ mice, which might be attributable to inflammation via other DNA-sensing pathways. Taken together, data clearly indicated that STING was implicated in the pathogenesis of RA in CIA mice.

3.3. Preparation and characterization of PEI-PDA@C-176 NPs

Mesoporous PDA NPs were prepared after extracting pluronic F127 micellar templates. The obtained spherical PDA NPs were relatively small, with a well-defined mesoporous structure (Fig. 3A and B) and negatively charged on the surface (Fig. 3C). Due to the low solubility in water, C-176 can be deposited into the pores of PDA NPs. C-176 content in PDA NPs increased as the feeding concentration increased and reached the maximal concentration of 13.7% (Fig. 3D). Thus, we selected PDA@C-176 NPs with 10% C-176 for further experiments. C-176 loading did not lead to a significant change in the morphology (Fig. 3A), size distribution (Fig. 3B), and surface zeta potential (Fig. 3C) of PDA NPs. We further coated PEI molecules onto the PDA@C-176 NPs via physical adsorption. As expected, the level of PEI adsorption gradually increased as the feeding concentration of PEI increased but plateaued when it reached 80 μg/mL (Fig. 3E). PEI coating did not result in a significant change in morphology (Fig. 3A) and size (Fig. 3B) of the particles, but the surface of PEI-PDA@C-176 NPs became positively charged (Fig. 3C). Additionally, PEI coating did not affect the sustained release of C-176 from PDA@C-176 NPs (Fig. 3F), suggesting that PEI coating had good permeability for small molecules such as C-176.

The associations between DNA and various NPs were examined by agarose gel electrophoresis (Fig. 3G). Compared to the naked DNA and PDA@C-176-treated DNA, the movement of PEI-PDA@C-176 NPs-treated DNA was almost completely retarded (>90%, Fig. 3G), suggesting there was a strong binding effect between PEI-PDA@C-176 NPs and DNA. As DNA was adsorbed by the PDA NPs and retained in the loading well, and the PDA NPs had strong light-absorbing ability, no DNA signal was observed in the lane with PDA NPs materials. Most DNA (>90%) was adsorbed by PEI-PDA@C-176 NPs when the DNA concentration was <25 μg/mL (Fig. 3H), suggesting a strong DNA adsorbing ability of the compound, and that PEI-PDA@C-176 NPs can adsorb and scavenge DNA at a ratio of approximately 1:50. The prolonged incubation time of DNA and NPs could increase DNA-binding efficiency but reached a plateau after 2-h incubation (Fig. 3I). Overall, results suggested a successful loading of the STING antagonist C-176 in the PDA NPs for sustained release and PEI-PDA NPs could efficiently adsorb cell-free DNA. The synthesized PEI-PDA@C-176 NPs thus might have synergistic effects on inhibiting the STING pathway.

The retention of PEI-PDA NPs under healthy and RA conditions was evaluated by intra-articular injection of Cy5-labeled PEI-PDA NPs in knee joints of normal and CIA mice (Fig. S2A). With infrared fluorescence imaging devices, Cy5-labeled NPs were detected to obtain drug retention information. After a single injection to the knee joint of the CIA model mice, the fluorescent signal of Cy5-labeled PEI-PDA NPs was significantly higher than that of Cy5-labeled PDA NPs on both days 3 and 7 (Fig. S2B), indicating that PEI coating increased the affinity of PDA NPs for RA joints.

The influence of PDA NPs on cell viability was investigated with live/dead cell staining assay and CCK8 assay. After the treatment with PDA NPs, the proportion of viable cells did not significantly change, indicating good biocompatibility (Figs. S3A–C). We performed live/dead cell viability experiments after incubation in 1 μg/mL PDA NPs for 1, 3, 5 days and in 1, 5, 10 μg/mL PDA NPs for 1 day, respectively (Fig. S4). After treated with NPs at various concentrations and different incubation times, the proportion of viable cells did not change significantly, indicating good biocompatibility of the synthesized materials. The systemic toxicity of PDA NPs was also evaluated in mice. During the experimental period, there was no difference in body weight for mice in various groups (Fig. S5A). Blood erythrocytes, leukocytes, and hemoglobin (Figs. S5B–D) also did not significantly differ among groups. No

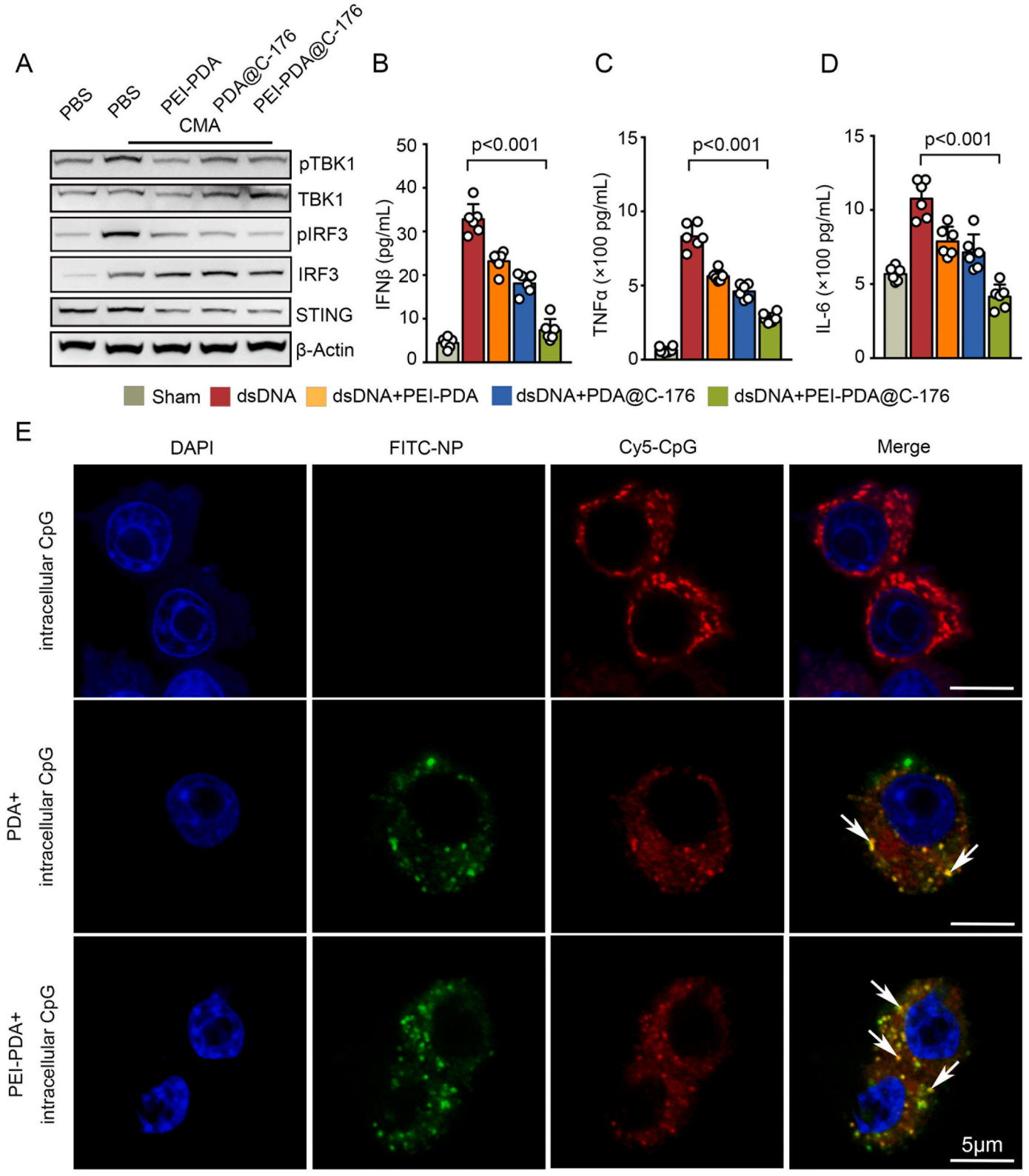

Fig. 4. PEI-PDA@C-176 NPs inhibited STING pathway via scavenging dsDNA. (**A**) Representative immunoblotting of pTBK1, TBK1, pIRF3, IRF3, and STING in BMDMs after indicated treatments (n = 6 independent experiments), using β-Actin as control. ELISA of (B) IFNβ, (**C**) TNFα and (**D**) IL-6 revealed that PEI-PDA@C-176 NPs significantly inhibited dsDNA-induced IFNβ, TNFα and IL-6 secretion in human primary fibroblast-like synoviocytes. (**E**) Intracellular colocalization of dsDNA (red) with PDA and PEI-PDA NPs (green) in RAW264.7 cells. As indicated with white arrows, co-localization of dsDNA and PDA NPs showed up as yellow spots. Scale bars: 5 μm.

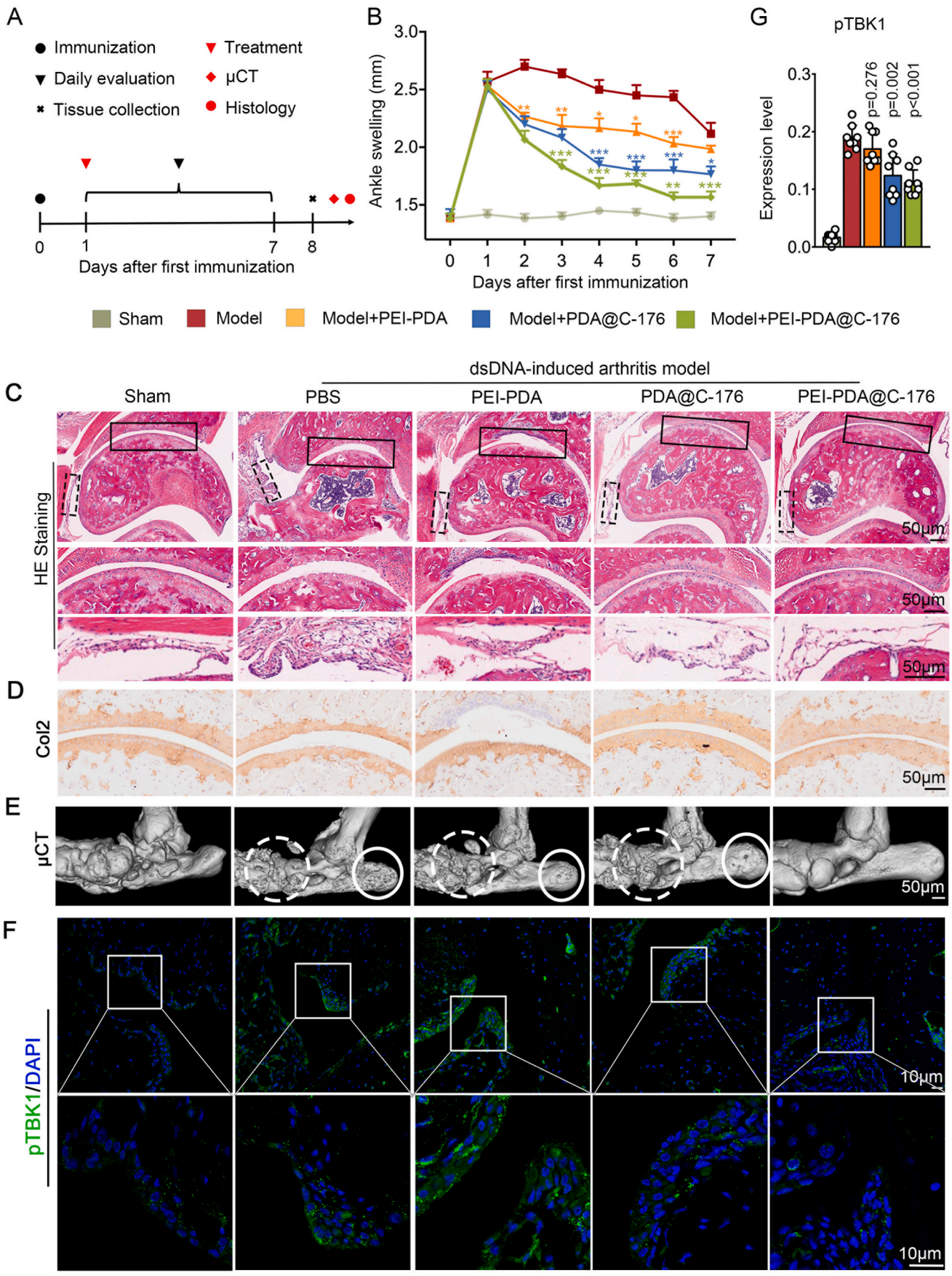

(caption on next page)

Fig. 5. PEI-PDA@C-176 NPs alleviated pathological features in dsDNA-induced acute arthritis. (**A**) Experimental schedule. (**B**) The diameter of the right ankle joints were measured to assess joint swelling after indicated treatment (n = 8). (**C**) Representative HE staining of the ankle joints, articular cartilage (solid frame), and synovium (dotted frame) from mice after indicated treatments (n = 8). (**D**) Representative immunohistochemistry of collagen II in ankle cartilage from mice after indicated treatments. (**E**) Representative μCT images of the ankle joints demonstrated bone destruction of various degrees in the calcaneus (white circle) and plantar joint (dotted circle). (**F**) Representative immunofluorescent staining of pTBK1 (green) in synovium of the ankle joints. (**G**) Quantitation of pTBK1 expression level (pixels per unit area) demonstrated that PEI-PDA@C-176 NP treatment reduced pTBK1 expression in the synovium. Statistical analysis is performed in comparison to the model group. *P < 0.05, **P < 0.01 and ***P < 0.001. Scale bars: 50 μm (**C**, **D**, and **E**) and 10 μm (**F**), respectively.

obvious morphological changes were observed in the major organs, including the liver, kidney, lung, spleen and heart (Fig. S5E), suggesting minimal systemic toxicity of PDA NPs, if any. Collectively, data suggested that PEI-PDA@C-176 NPs exhibited high biocompatibility and, thus, were suitable for therapeutic use.

3.4. PEI-PDA@C-176 NPs inhibited the STING pathway and dsDNA-induced inflammation

The STING agonist 10-carboxymethyl-9-acridanone (CMA) could bind to STING and trigger inflammatory responses through the TBK1/IRF3 axis. As a first step to evaluate the therapeutic efficacy of PEI-PDA@C-176 NPs, we investigated its effects on CMA-induced STING activation in BMDMs. While PDA@C-176 NPs reduced the expression level of pTBK1 and pIRF3 to 71% and 22.3%, respectively, PEI-PDA@C-176 NPs further reduced the expression of pTBK1 and pIRF3 to 31.6% and 14.9%, respectively (Fig. 4A, Figs. S6A–E). Besides, treatment with PEI-PDA@C-176 NPs suppressed the dsDNA-induced STING activation, significantly lowering IFNβ cytokine release (Fig. 4B). Results indicated that PEI-PDA@C-176 NPs had a stronger effect on STING inhibition than other formulations.

Then, we examined whether PEI-PDA@C-176 NPs could inhibit dsDNA-induced inflammatory responses. Using ELISA, we found that dsDNA-induced overexpression of TNF-α was significantly inhibited by 32%, 44.6%, and 71.4% in the presence of PEI-PDA, PDA@C-176, and PEI-PDA@C-176 NPs, respectively (Fig. 4C). Similarly, the production of IL-6 was also decreased by 26.8%, 33.7% and 61.4% in the presence of PEI-PDA, PDA@C-176 and PEI-PDA@C-176 NPs, respectively (Fig. 4D). Results demonstrated that PEI-PDA@C-176 NPs treatment could reduce the dsDNA-induced secretion of inflammatory cytokines.

Colocalization of PDA NPs and CpG in RAW264.7 cells was then studied (Fig. 4E). The colocalization ratio of FITC-labeled PEI-PDA NPs (green) with Cy5-labeled CpG (red) was significantly higher than that of PDA NPs (Fig. 4E), suggesting that PEI-coated PDA NPs obtained a strong dsDNA-binding capability. dsDNA clearance capability of PEI-PDA NPs was then investigated with immunostaining. Cell-free dsDNA was significantly decreased after the treatment with PDA and PEI-PDA NPs (Fig. S7A). There was a 3.4-fold and 6.7-fold decrease in the fluorescence intensity of dsDNA after PDA and PEI-PDA NP treatments respectively, indicating that PEI-PDA NPs had a strong capability of scavenging dsDNA.

3.5. PEI-PDA@C-176 NPs suppressed the STING signaling and alleviated inflammation in dsDNA-induced arthritis

Encouraged by the effect of PEI-PDA@C-176 NPs on modulating STING activation and inflammation *in vitro*, we further explored their effect in a mice model of dsDNA-induced acute arthritis (Fig. 5A). Both PEI-PDA and PDA@C-176 NP treatments relieved ankle swelling, and mice treated with PEI-PDA@C-176 NPs had quicker and greater alleviation in ankle swelling than those treated with other NPs (Fig. 5B).

In histological analysis, synovial lining hyperplasia was significantly alleviated in model mice treated with PEI-PDA@C-176 NPs (Fig. 5C). In mice treated with PEI-PDA@C-176, the histological score for synovitis was decreased to 0.9, which was significantly lower than that of mice treated with PEI-PDA (2.2) and PDA@C-176 (1.8) (Fig. S8A).

To assess cartilage destruction, which is another important RA pathology, HE staining (Fig. 5C) and immunohistochemical (IHC) staining of collagen II (Fig. 5D) were performed. Notably, PEI-PDA NPs alone did not appreciably affect cartilage destruction, while PDA@C-176 and PEI-PDA@C-176 NP treatments considerably alleviated cartilage destruction (Fig. 5C and D). After PEI-PDA@C-176 NP treatment, the histological score for cartilage destruction decreased to 0.8, which was significantly lower than those in the other groups (Fig. S8B).

μCT revealed that bone mineral density in mice treated with PEI-PDA@C-176 increased to a level close to that in the sham group. While there were significant bone defects in the calcaneus (solid circle) and cuneiform bones (dot circle) in the model mice treated with PBS or other NPs, bone destruction was barely noticed in the model mice treated with PEI-PDA@C-176 NPs (Fig. 5E), as was further evidenced by significantly lower histological score of bone erosion in this group (Fig. S8C).

Immunofluorescence staining further demonstrated that while PEI-PDA NP treatment did not affect STING activation (Fig. 5F and G), PEI-PDA@C-176 NP treatment significantly reduced the expression of pTBK1 by 45.3% (Fig. 5F and G). Taken together, results indicated that PEI-PDA@C-176 NPs suppressed the STING signaling and attenuated pathologies in the mice model of dsDNA-induced arthritis.

3.6. PEI-PDA@C-176 NPs suppressed the STING signaling and alleviated inflammation in the CIA model

The therapeutic potential of PEI-PDA@C-176 NPs was further examined in the CIA model (Fig. 6A), which is regarded as the gold standard for experimental RA due to its systematic immune responses. The CIA model mice gradually developed arthritis, and their clinical score reached a maximum of 6.7 points on day 24 after the first immunization (Fig. 6B). While mice treated with PDA@C-176 showed reduced arthritis, those treated with PEI-PDA@C-176 NPs showed a greater decrease in the clinical score ($p < 0.001$, Fig. 6B). After PEI-PDA@C-176 NPs treatment, the diameter of the inflamed knee joint decreased to 1.07 mm, which was significantly lower than those in the model mice (1.52 mm) and PEI-PDA treated mice (1.41 mm) (Fig. 6C).

Synovitis which is a key indicator of RA was observed in the CIA model mice and PEI-PDA treated mice with features including synovial hyperplasia and immune cell infiltration (Fig. 6D). Synovitis was effectively controlled after PEI-PDA@C-176 NPs treatment, and the histological score was 0.9 (Fig. 6G), which was significantly lower than that in the model mice (1.8) and PEI-PDA treated mice (1.3). Cartilage destruction was then evaluated as another typical sign of RA. PEI-PDA NPs treated mice exhibited a cartilage pattern similar to that in the model mice, with apparent cartilage erosion and reduced cartilage thickness (Fig. 6D). After PEI-PDA@C-176 NPs treatment, however, the knee joint displayed only minor signs of cartilage degradation (Fig. 6D), and the histological score was markedly lower than that in mice treated with PBS or other NPs (Fig. 6H). Subchondral bone damage as a late RA pathology was further assessed with μCT. While there was bone destruction of various degrees in the distal end of the femur (circle) in the CIA model mice (Fig. 6E), there was only slight bone damage in the CIA mice treated with PEI-PDA@C-176 NPs ($p < 0.001$, Fig. 5E and I).

Injection of PEI-PDA@C-176 NPs, but not PEI-PDA NPs, inhibited STING activation (Fig. 6F and J). In mice treated with PDA@C-176 and PEI-PDA@C-176 NPs, the pTBK1 expression decreased to 56.1% and 51.8%, respectively (Fig. 6F and J). Taken together, results indicated that PEI-PDA@C-176 NPs could suppress the STING signaling and alleviate articular inflammation in the CIA model mice. PEI coating and

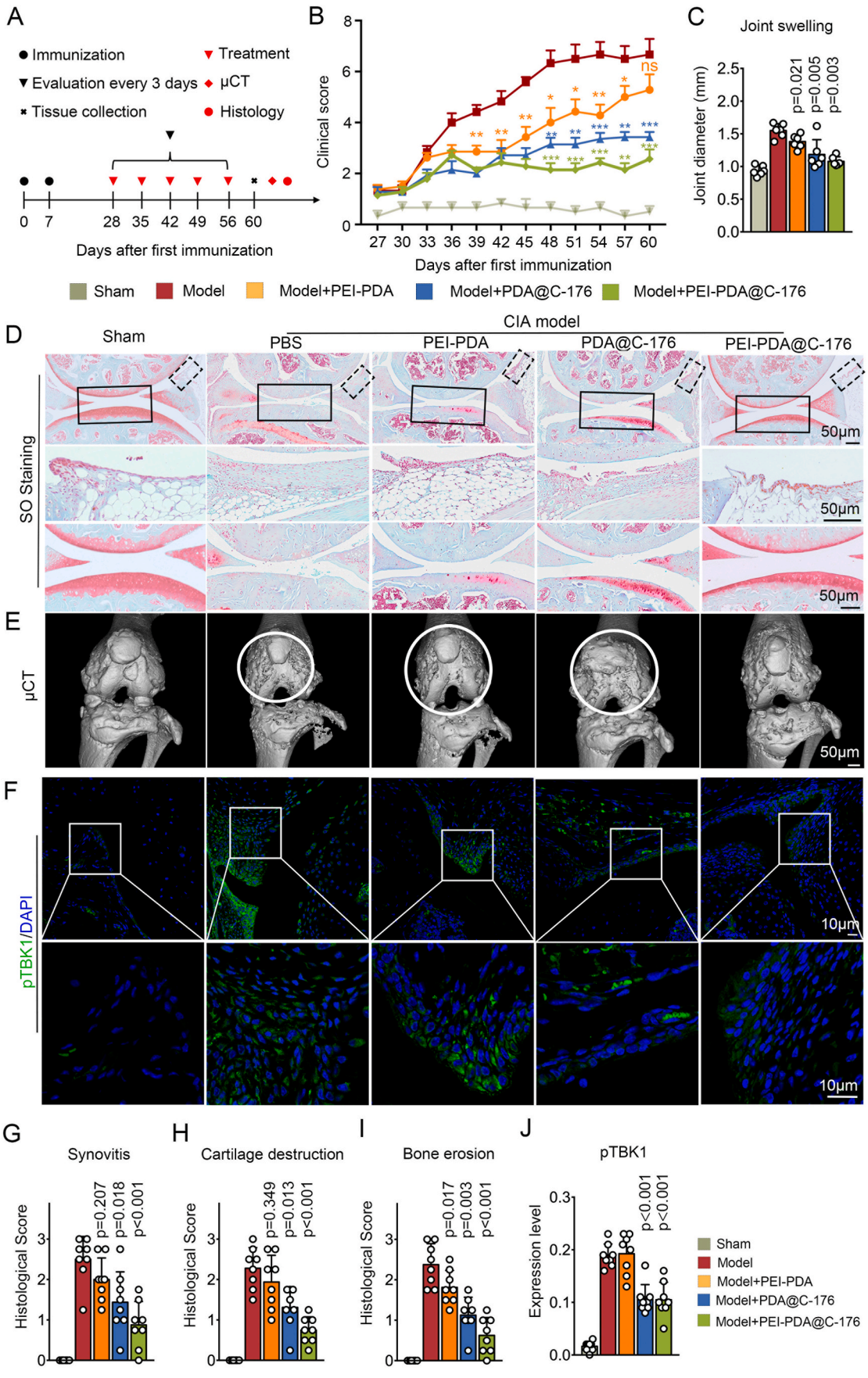

(caption on next page)

Fig. 6. PEI-PDA@C-176 NPs attenuated pathological features in CIA model mice. (**A**) Experimental schedule. (**B**) Clinical scores were evaluated every 3 days (n = 8 mice per group). (**C**) The diameter of the right knee joint was measured to assess joint swelling for CIA model mice after indicated treatments. (**D**) Representative SO staining of the right knee joints, articular cartilage (solid frame) and synovium (dotted frame) from sham and CIA model mice subjected to intra-articular injection of indicated NPs, respectively. (**E**) Representative μCT images of the right knee joints revealed bone erosion of various degrees in the distal end of the femur (circle). (**F**) Representative immunofluorescent staining of pTBK1 (green) of the synovium from mice after indicated treatments. Histological scores for the (**G**) synovitis, (**H**) cartilage destruction and (**I**) bone erosion revealed that PEI-PDA@C-176 NPs significantly alleviated arthritis pathological changes in CIA model mice. (**J**) Quantitation of pTBK1 expression level (pixels per unit area) demonstrated that PEI-PDA@C-176 NPs reduced pTBK1 expression in synovium. Statistical analysis was performed in comparison to CIA model mice treated with PBS. *P < 0.05, **P < 0.01 and ***P < 0.001. ns, not significant. Scale bars: 50 μm (**D** and **E**) and 10 μm (**F**), respectively.

C-176 loading enabled PEI-PDA@C-176 NPs to exert a strong inhibitory effect on RA inflammation and pathogenesis.

3.7. PEI-PDA@C-176 NPs alleviated inflammation through the STING pathway

To further understand the mechanism underlying the therapeutic effect of PEI-PDA@C-176 NPs in treating RA, the newly developed NPs were applied to *Sting1*$^{+/-}$ mice (Fig. 7A). After modeling, *Sting1*$^{+/-}$ mice showed minor joint swelling, and their clinical score reached a maximum of 3 points. In *Sting1*$^{+/-}$ mice, PDA@C-176 treatment did not reduce the clinical score, while PEI-PDA@C-176 NPs treatment reduced the clinical score by only 1.5 points (Fig. 7B). No difference in the diameter of the knee was observed among CIA modeled *Sting1*$^{+/-}$ mice treated with PBS or various NPs (Fig. 7C).

Similarly, there was no significant difference in synovitis in CIA modeled *Sting1*$^{+/-}$ mice after various treatments (Fig. 7D and G). SO staining also revealed that cartilage destruction in CIA modeled *Sting1*$^{+/-}$ mice remained after treatment with PEI-PDA, PDA@C-176, or PEI-PDA@C-176 NPs (Fig. 7D and H). The μCT images demonstrated that bone destruction, which is highlighted in a circle, was not changed after treatment with PEI-PDA, PDA@C-176 or PEI-PDA@C-176 NPs (Fig. 7E and I).

The STING activation was investigated in CIA-modeled *Sting1*$^{+/-}$ mice (Fig. 7F and J). As expected, immunofluorescence staining revealed that *Sting1*$^{+/-}$ mice did not show reduced pTBK1 expression after the treatment with PEI-PDA, PDA@C-176 or PEI-PDA@C-176 NPs. Findings suggested that PEI-PDA@C-176 NPs might inhibit RA inflammation via the STING signaling.

4. Discussion

In this study, we found there were significant cell-free dsDNA accumulation and STING activation in the synovial tissues of human RA patients and RA model mice. With *STING* knockout mice, we found that the STING pathway was critical for inflammation and joint damage in RA. Given these findings and the fact that dsDNA is a specific stimulus for STING, we developed PDA-based NPs to simultaneously capture dsDNA and deliver STING antagonist C-176. The fabricated PEI-PDA@C-176 NPs, which has synergetic effects on STING inhibition, could reduce the secretion of dsDNA-induced inflammatory cytokines in macrophages. Intra-articular administration of PEI-PDA@C-176 NPs effectively reduced joint damage in both the dsDNA-induced arthritis model and CIA model. Together, these findings illustrated that inhibition of the STING pathway by dsDNA adsorption and STING antagonist might be a promising therapeutic strategy for treating RA.

The evolution of RA follows a sequential process of joint inflammation and damage, which is irreversible in most cases [41], and the mechanism underlying this sequential process has not been fully clarified [42]. However, it is clear that the transition from the recognition of modified antigens to metabolic and DNA instability-induced immune cell invasion and chronic synovitis is an important checkpoint [41]. In this study, we found that the STING pathway sensed DNA damage and upregulated the secretion of inflammatory cytokines, such as TNF-α in macrophages. While TNF-α is secreted from synovial immune cells, such as macrophages, TNF-α receptors are expressed in both macrophages and synovial fibroblasts [43]. Consequently, this study raised the possibility that STING-induced synthesis of inflammatory cytokines bypassed the checkpoint of immune tolerance and, thus, promoted inflammation. Further, communication between immune cells and their surrounding extracellular matrix in the synovium microenvironment is essential for the maintenance of homeostasis in joint tissues [44]. As cytokines are connectors between abnormal adaptive immune responses and adverse tissue remodeling in RA [45,46], STING inhibition might ameliorate structural deficiencies by reducing the aberrant immune responses in RA synovial environment [41]. Our findings suggested that targeting upstream immune checkpoints could re-engineer the immune system and attenuate the progression of RA before irreversible tissue damage occurred.

The STING pathway can be triggered by various cytosolic dsDNA species, regardless of their origins and sequences [47]. As a result, STING plays an essential role in autoimmune diseases [48]. Different from other innate immune pathways which are pathogen-specific, cGAS recognizes a wide range of DNA species, including dsDNA derived from pathogens and dsDNA of self-origins, such as damaged mitochondrial DNA (mtDNA) and leaked/damaged nuclear DNA from the cytosol or cell debris [49,50]. As such, STING exhibits diverse regulatory functions in various cellular progresses, and hyperactivation of the cGAS/STING signaling is essential in the development of autoimmune diseases. In RA, insufficient DNA repair leads to the accumulation of damaged DNA in the nucleus. Unrepaired DNA damage might promote immune cell pyroptosis and premature aging [51–53]. However, as a well-recognized DNA sensor [47], STING has been less studied in RA, and the effect of inhibiting STING remains unknown. In this study, the accumulation of damaged dsDNA in RA synovial tissues activated the STING signaling, which led to tissue damage and inflammation, suggesting that STING might be an important connector between DNA instability and RA pathology. More studies are needed to further understand the causative roles of the cGAS-STING pathway in RA.

As the cGAS-STING signaling is important in inflammatory diseases, several methods targeting different stages in STING signaling have been proposed [10–12]. Astin C, a cyclopentapeptide isolated from a medicinal composite, can inhibit cGAS-STING signaling in the presence of cytosolic DNAs and thus, weaken autoimmune responses [54]. Also, cGAS antagonists have been developed to interfere with the initial step of STING activation by competing with cGAS binding [55–57], although such an approach has off-target problems due to the universal protein–DNA binding mechanism. On the other hand, small molecules targeting protein palmitoylation can affect the interactions between STING and lipids and proteins, thus, covalently inhibiting STING [58]. The developed STING inhibitors can occupy the cyclic dinucleotide (CDN)-binding site and, thus, attenuate pathologies in many inflammatory diseases [19–21]. Inhibitors in the CDN-binding pocket strongly reduce systemic inflammation and protect mice from sterile inflammatory diseases [24]. Yet, to our knowledge, all studies have used only one strategy to inhibit STING activation.

In this study, we developed PEI-PDA@C-176 NPs, which could simultaneously adsorb dsDNA and inhibit STING palmitoylation. C-176 is a newly developed nitrofuran analog that covalently targets Cys91 and, therefore, inhibits the palmitoylation of STING [18]. C-176 had a prolonged effect on STING inhibition and suppressed STING-associated autoinflammation *in vivo* without obvious signs of toxicity. Besides, we

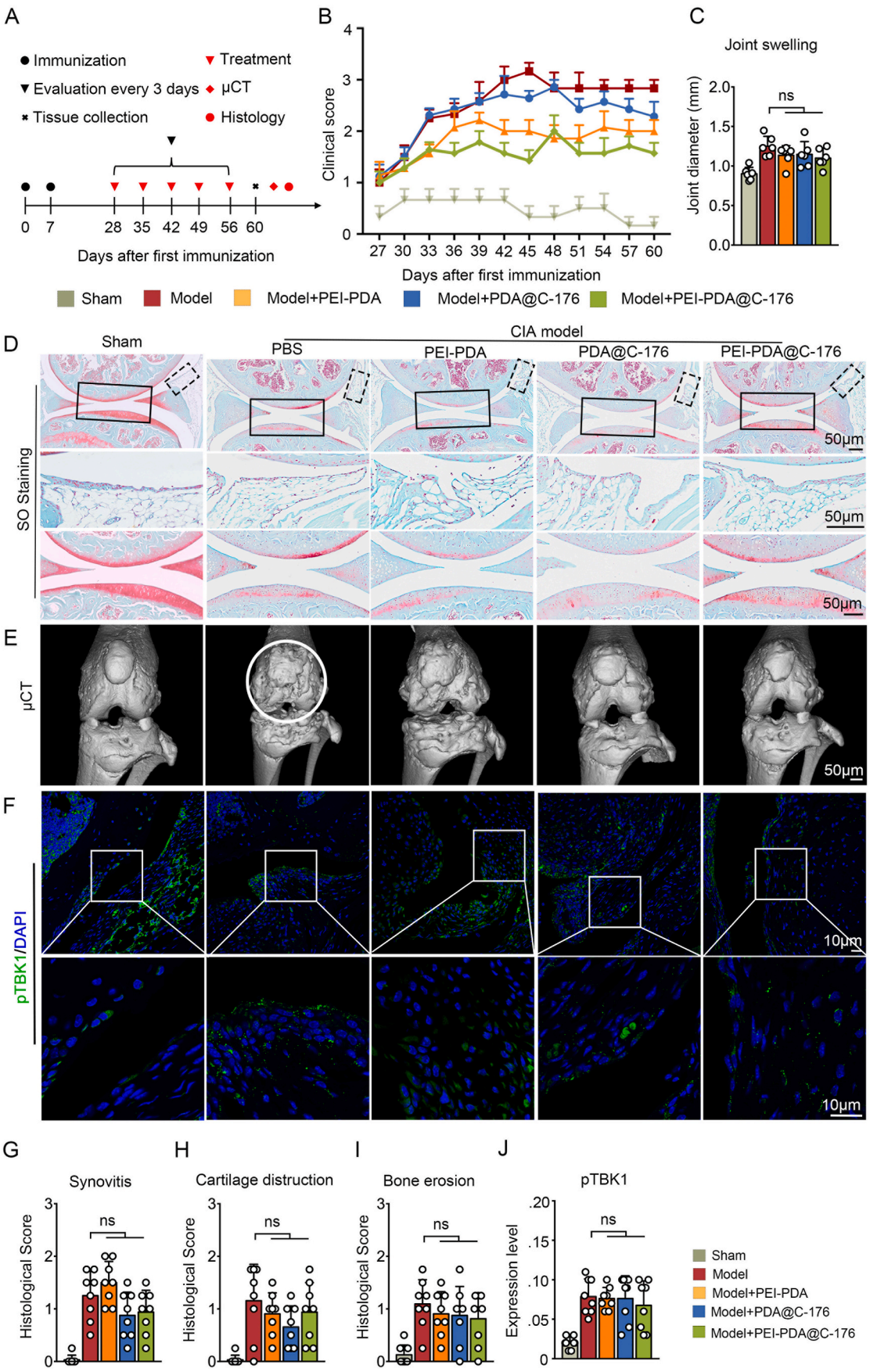

(caption on next page)

Fig. 7. PEI-PDA@C-176 NPs alleviated CIA pathological changes via the STING pathway. (**A**) Experimental schedule. (**B**) Clinical score was evaluated every 3 days (n = 8). (**C**) The diameter of the right knee joints was measured to assess joint swelling for *Sting1*$^{+/-}$ mice after indicated treatments. (**D**) Representative SO staining of the right knee joints, articular cartilage (solid frame), and synovium (dotted frame) from *Sting1*$^{+/-}$ mice after indicated treatments. (**E**) Representative μCT images of the right knee joints from *Sting1*$^{+/-}$ mice demonstrated bone destruction in the distal end of the femur (circle). (**F**) Representative immunofluorescent staining of pTBK1 (green) in the synovium from *Sting1*$^{+/-}$ mice after indicated treatments. Histological scores for the (**G**) synovitis, (**H**) cartilage destruction and (**I**) bone erosion revealed that PEI-PDA@C-176 did not affect pathological changes in CIA modeled *Sting1*$^{+/-}$ mice. (**J**) Statistical analysis of pTBK1 expression (pixels per unit area) demonstrated that STING activation in CIA modeled *Sting1*$^{+/-}$ mice was not affected after different treatment. Statistical analysis was performed in comparison to CIA model mice treated with PBS. ns, not significant. Scale bars: 50 μm (**D** and **E**) and 10 μm (**F**), respectively.

developed PDA-based NPs as the carrier for C-176 because this compound has good biocompatibility and high drug loading capacity [59–61] and has been used in the diagnosis and treatment of cancer and eye disease [62,63]. In this study, the developed PDA@C-176 NPs achieved better therapeutic effects than other formulations with single functions both *in vivo* and *in vitro*. These findings suggested that simultaneous inhibition of various stages of STING signaling can have a synergetic effect of STING inhibition and thus improve the therapeutic effect with a reduced drug dose. Such a strategy also shows potentials in a wide range of therapeutic applications. Nevertheless, there are several future work directions. STING activation was only examined in RA synovial specimens from RA patients who were in the late stage of RA. Due to limitations in clinical practice, we were not able to collect synovium at the early stage of RA and thus, the role of STING in early RA remains unknown. We used STING knockout mice but not conditional knockout mice to evaluate the role of STING in PEI-PDA@C-176 NP treatment. As various types of cells are involved in the pathology of RA [41,64,65], it is possible that the therapeutic effect of PEI-PDA@C-176 NPs was partially attributed to other types of cells. Additionally, PEI-PDA@C-176 NPs were found to treat RA by scavenging dsDNA. dsDNA can induce inflammatory responses through various DNA-sensing pathways [66,67], such as the AIM2 pathway [68]. These pathways may also play an important role in the treatment of PEI-PDA@C-176.

5. Conclusion

In this study, we demonstrated the feasibility of targeting the STING signaling to block the initiation of RA pathology. The fabricated PEI-PDA@C-176 NPs were highly biocompatible and could simultaneously adsorb the STING stimulus (dsDNA) and inhibit STING palmitoylation. With such a synergetic effect of inhibiting the STING signaling, PEI-PDA@C-176 NPs showed a remarkable effect on alleviating RA inflammation and pathology. Such comprehensive studies shed light on the development of disease-modifying drugs for RA and other autoimmune diseases.

Funding

This work was supported by the National Natural Science Foundation of China (81772382, 22161132027 and 82102599), the Key Research Program in Zhejiang Province, Science Technology Department of Zhejiang Province (2020C03042) and the Starry Night Science Fund of Zhejiang University Shanghai Institute for Advanced Study (SN-ZJU-SIAS-006).

Data availability

All data needed to evaluate the conclusions in the paper are present in the paper and/or the Supplementary Materials. Additional data related to this paper may be requested from the authors.

Credit authorship contribution statement

Haotian Shen: Conceptualization, Methodology, Validation, Formal analysis and Writing - Original Draft. Lulu Jin: Methodology, Validation, Investigation. Qiangqiang Zheng: Methodology, Validation, and Formal analysis. Ziqiang Ye: Methodology. Zongyou Pan: Conceptualization, Methodology and Funding acquisition. Linxiang Cheng: Methodology, Validation. Wenduo Liu: Methodology. Zhengwei Mao: Conceptualization, Methodology, Supervision, Writing - Review & Editing, and Funding acquisition. Yue Wang: Supervision, Writing - Review & Editing, and Funding acquisition.

Ethics approval and consent to participate

All experiments related to human samples were approved by the ethical review board at the First Affiliated Hospital, Zhejiang University School of Medicine (ethic code: ZDYY-20210136B). All animal studies were performed with the approval of the ethical review board at the First Affiliated Hospital, Zhejiang University School of Medicine (ethic code: ZDYY-2021-917). The animal experiment guidance from the ethical committee and the guide for care and use of laboratory animals from NIH were followed during the whole experiment course.

Declaration of competing interest

The authors declare that they have no known competing financial interests or personal relationships that could have appeared to influence the work reported in this paper.

Appendix A. Supplementary data

Supplementary data to this article can be found online at https://doi.org/10.1016/j.bioactmat.2022.12.001.

References

[1] S. Safiri, A.A. Kolahi, D. Hoy, E. Smith, D. Bettampadi, M.A. Mansournia, A. Almasi-Hashiani, A. Ashrafi-Asgarabad, M. Moradi-Lakeh, M. Qorbani, G. Collins, A.D. Woolf, L. March, M. Cross, Global, regional and national burden of rheumatoid arthritis 1990-2017: a systematic analysis of the Global Burden of Disease study 2017, Ann. Rheum. Dis. (2019).

[2] Y.M. Chiu, Y.P. Lu, J.L. Lan, D.Y. Chen, J.D. Wang, Lifetime risks, life expectancy, and health care expenditures for rheumatoid arthritis: a nationwide cohort followed up from 2003 to 2016, Arthritis Rheumatol. 73 (5) (2021) 750–758.

[3] M. Schoels, R. Knevel, D. Aletaha, J.W.J. Bijlsma, F.C. Breedveld, D.T. Boumpas, G. Burmester, B. Combe, M. Cutolo, M. Dougados, P. Emery, D. van der Heijde, T. W.J. Huizinga, J. Kalden, E.C. Keystone, T.K. Kvien, E. Martin-Mola, C. Montecucco, M. de Wit, J.S. Smolen, Evidence for treating rheumatoid arthritis to target: results of a systematic literature search, Ann. Rheum. Dis. 69 (4) (2010) 638–643.

[4] J.S. Smolen, R.B.M. Landewe, J.W.J. Bijlsma, G.R. Burmester, M. Dougados, A. Kerschbaumer, I.B. McInnes, A. Sepriano, R.F. van Vollenhoven, M. de Wit, D. Aletaha, M. Aringer, J. Askling, A. Balsa, M. Boers, A.A. den Broeder, M.H. Buch, F. Buttgereit, R. Caporali, M.H. Cardiel, D. De Cock, C. Codreanu, M. Cutolo, C. J. Edwards, Y. van Eijk-Hustings, P. Emery, A. Finckh, L. Gossec, J.E. Gottenberg, M.L. Hetland, T.W.J. Huizinga, M. Koloumas, Z. Li, X. Mariette, U. Muller-Ladner, E.F. Mysler, J.A.P. da Silva, G. Poor, J.E. Pope, A. Rubbert-Roth, A. Ruyssen-Witrand, K.G. Saag, A. Strangfeld, T. Takeuchi, M. Voshaar, R. Westhovens, D. van der Heijde, EULAR recommendations for the management of rheumatoid arthritis with synthetic and biological disease-modifying antirheumatic drugs: 2019 update, Ann. Rheum. Dis. 79 (6) (2020) 685–699.

[5] P. Conigliaro, P. Triggianese, E. De Martino, G.L. Fonti, M.S. Chimenti, F. Sunzini, A. Viola, C. Canofari, R. Perricone, Challenges in the treatment of rheumatoid arthritis, Autoimmun. Rev. 18 (7) (2019) 706–713.

[6] M. Pirmohamed, S. James, S. Meakin, C. Green, A.K. Scott, T.J. Walley, K. Farrar, B.K. Park, A.M. Breckenridge, Adverse drug reactions as cause of admission to hospital: prospective analysis of 18 820 patients, BMJ 329 (7456) (2004) 15–19.

[7] H. Manabe, Y. Nasu, T. Komiyama, T. Furumatsu, A. Kitamura, S. Miyazawa, Y. Ninomiya, T. Ozaki, H. Asahara, K. Nishida, Inhibition of histone deacetylase down-regulates the expression of hypoxia-induced vascular endothelial growth factor by rheumatoid synovial fibroblasts, Inflamm. Res. 57 (1) (2008) 4–10.

[8] G.R. Burmester, J.E. Pope, Novel treatment strategies in rheumatoid arthritis, Lancet 389 (10086) (2017) 2338–2348.

[9] S.J. Chen, G.J. Lin, J.W. Chen, K.C. Wang, C.H. Tien, C.F. Hu, C.N. Chang, W. F. Hsu, H.C. Fan, H.K. Sytwu, Immunopathogenic mechanisms and novel immune-modulated therapies in rheumatoid arthritis, Int. J. Mol. Sci. 20 (6) (2019).

[10] S. Gluck, B. Guey, M.F. Gulen, K. Wolter, T.W. Kang, N.A. Schmacke, A. Bridgeman, J. Rehwinkel, L. Zender, A. Ablasser, Innate immune sensing of cytosolic chromatin fragments through cGAS promotes senescence, Nat. Cell Biol. 19 (9) (2017) 1061–1070.

[11] L. Galluzzi, A. Lopez-Soto, S. Kumar, G. Kroemer, Caspases connect cell-death signaling to organismal homeostasis, Immunity 44 (2) (2016) 221–231.

[12] H. Yang, H. Wang, J. Ren, Q. Chen, Z.J. Chen, cGAS is essential for cellular senescence, Proc. Natl. Acad. Sci. U. S. A. 114 (23) (2017) E4612–E4620.

[13] Y. Liu, A.A. Jesus, B. Marrero, D. Yang, S.E. Ramsey, G.A.M. Sanchez, K. Tenbrock, H. Wittkowski, O.Y. Jones, H.S. Kuehn, C.R. Lee, M.A. DiMattia, E.W. Cowen, B. Gonzalez, I. Palmer, J.J. DiGiovanna, A. Biancotto, H. Kim, W.L. Tsai, A. M. Trier, Y. Huang, D.L. Stone, S. Hill, H.J. Kim, C. St Hilaire, S. Gurprasad, N. Plass, D. Chapelle, I. Horkayne-Szakaly, D. Foell, A. Barysenka, F. Candotti, S. M. Holland, J.D. Hughes, H. Mehmet, A.C. Issekutz, M. Raffeld, J. McElwee, J. R. Fontana, C.P. Minniti, S. Moir, D.L. Kastner, M. Gadina, A.C. Steven, P. T. Wingfield, S.R. Brooks, S.D. Rosenzweig, T.A. Fleisher, Z. Deng, M. Boehm, A. S. Paller, R. Goldbach-Mansky, Activated STING in a vascular and pulmonary syndrome, N. Engl. J. Med. 371 (6) (2014) 507–518.

[14] D.L. Burdette, R.E. Vance, STING and the innate immune response to nucleic acids in the cytosol, Nat. Immunol. 14 (1) (2013) 19–26.

[15] M. Motwani, S. Pawaria, J. Bernier, S. Moses, K. Henry, T. Fang, L. Burkly, A. Marshak-Rothstein, K.A. Fitzgerald, Hierarchy of clinical manifestations in SAVI N153S and V154M mouse models, Proc. Natl. Acad. Sci. U. S. A. 116 (16) (2019) 7941–7950.

[16] T. Taguchi, K. Mukai, Innate immunity signalling and membrane trafficking, Curr. Opin. Cell Biol. 59 (2019) 1–7.

[17] A. Ablasser, Z.J. Chen, cGAS in action: expanding roles in immunity and inflammation, Science 363 (6431) (2019).

[18] S.M. Haag, M.F. Gulen, L. Reymond, A. Gibelin, L. Abrami, A. Decout, M. Heymann, F.G. van der Goot, G. Turcatti, R. Behrendt, A. Ablasser, Targeting STING with covalent small-molecule inhibitors, Nature 559 (7713) (2018) 269–273.

[19] B. Wu, M.M. Xu, C. Fan, C.L. Feng, Q.K. Lu, H.M. Lu, C.G. Xiang, F. Bai, H.Y. Wang, Y.W. Wu, W. Tang, STING inhibitor ameliorates LPS-induced ALI by preventing vascular endothelial cells-mediated immune cells chemotaxis and adhesion, Acta Pharmacol. Sin. (2021).

[20] P.T. Pham, D. Fukuda, S. Nishimoto, J.R. Kim-Kaneyama, X.F. Lei, Y. Takahashi, T. Sato, K. Tanaka, K. Suto, Y. Kawabata, K. Yamaguchi, S. Yagi, K. Kusunose, H. Yamada, T. Soeki, T. Wakatsuki, K. Shimada, Y. Kanematsu, Y. Takagi, M. Shimabukuro, M. Setou, G.N. Barber, M. Sata, STING, a cytosolic DNA sensor, plays a critical role in atherogenesis: a link between innate immunity and chronic inflammation caused by lifestyle-related diseases, Eur. Heart J. 42 (42) (2021) 4336–4348.

[21] B. Han, X. Wang, P. Wu, H. Jiang, Q. Yang, S. Li, J. Li, Z. Zhang, Pulmonary inflammatory and fibrogenic response induced by graphitized multi-walled carbon nanotube involved in cGAS-STING signaling pathway, J. Hazard Mater. 417 (2021), 125984.

[22] Q. Guo, X. Chen, J. Chen, G. Zheng, C. Xie, H. Wu, Z. Miao, Y. Lin, X. Wang, W. Gao, X. Zheng, Z. Pan, Y. Zhou, Y. Wu, X. Zhang, STING promotes senescence, apoptosis, and extracellular matrix degradation in osteoarthritis via the NF-kappaB signaling pathway, Cell Death Dis. 12 (1) (2021) 13.

[23] M. Tansakul, A. Thim-Uam, T. Saethang, J. Makjaroen, B. Wongprom, T. Pisitkun, P. Pisitkun, Deficiency of STING promotes collagen-specific antibody production and B cell survival in collagen-induced arthritis, Front. Immunol. 11 (2020) 1101.

[24] Z. Hong, J. Mei, H. Guo, J. Zhu, C. Wang, Intervention of cGASSTING signaling in sterile inflammatory diseases, J. Mol. Cell Biol. (2022).

[25] N. Lohmann, L. Schirmer, P. Atallah, E. Wandel, R.A. Ferrer, C. Werner, J.C. Simon, S. Franz, U. Freudenberg, Glycosaminoglycan-based hydrogels capture inflammatory chemokines and rescue defective wound healing in mice, Sci. Transl. Med. 9 (386) (2017).

[26] Y. Peng, D. He, X. Ge, Y. Lu, Y. Chai, Y. Zhang, Z. Mao, G. Luo, J. Deng, Y. Zhang, Construction of heparin-based hydrogel incorporated with Cu5.4O ultrasmall nanozymes for wound healing and inflammation inhibition, Bioact. Mater. 6 (10) (2021) 3109–3124.

[27] H. Liang, B. Peng, C. Dong, L. Liu, J. Mao, S. Wei, X. Wang, H. Xu, J. Shen, H. Q. Mao, X. Gao, K.W. Leong, Y. Chen, Cationic nanoparticle as an inhibitor of cell-free DNA-induced inflammation, Nat. Commun. 9 (1) (2018) 4291.

[28] B. Peng, H. Liang, Y. Li, C. Dong, J. Shen, H.Q. Mao, K.W. Leong, Y. Chen, L. Liu, Tuned cationic dendronized polymer: molecular scavenger for rheumatoid arthritis treatment, Angew Chem. Int. Ed. Engl. 58 (13) (2019) 4254–4258.

[29] J. Wang, R. Li, H. Lin, Q. Qiu, M. Lao, S. Zeng, C. Wang, S. Xu, Y. Zou, M. Shi, L. Liang, H. Xu, Y. Xiao, Accumulation of cytosolic dsDNA contributes to fibroblast-like synoviocytes-mediated rheumatoid arthritis synovial inflammation, Int. Immunopharm. 76 (2019), 105791.

[30] F. Ying, J.P. Chalise, S.C. Narendra, M. Magnusson, Type I IFN protects against antigen-induced arthritis, Eur. J. Immunol. 41 (6) (2011) 1687–1695.

[31] T. Jiang, Y. Qiao, W. Ruan, D. Zhang, Q. Yang, G. Wang, Q. Chen, F. Zhu, J. Yin, Y. Zou, R. Qian, M. Zheng, B. Shi, Cation-free siRNA micelles as effective drug delivery platform and potent RNAi nanomedicines for glioblastoma therapy, Adv. Mater. 33 (45) (2021), e2104779.

[32] J. Kim, H.Y. Kim, S.Y. Song, S.H. Go, H.S. Sohn, S. Baik, M. Soh, K. Kim, D. Kim, H. C. Kim, N. Lee, B.S. Kim, T. Hyeon, Synergistic oxygen generation and reactive oxygen species scavenging by manganese ferrite/ceria Co-decorated nanoparticles for rheumatoid arthritis treatment, ACS Nano 13 (3) (2019) 3206–3217.

[33] R. Zampieri, A. Brozzetti, E. Pericolini, E. Bartoloni, E. Gabrielli, E. Roselletti, G. Lomonosoff, Y. Meshcheriakova, L. Santi, F. Imperatori, M. Merlin, E. Tinazzi, F. Dotta, L. Nigi, G. Sebastiani, M. Pezzotti, A. Falorni, L. Avesani, Prevention and treatment of autoimmune diseases with plant virus nanoparticles, Sci. Adv. 6 (19) (2020) eaaz0295.

[34] X. Chen, X. Zhu, L. Ma, A. Lin, Y. Gong, G. Yuan, J. Liu, A core-shell structure QRu-PLGA-RES-DS NP nanocomposite with photothermal response-induced M2 macrophage polarization for rheumatoid arthritis therapy, Nanoscale 11 (39) (2019) 18209–18223.

[35] R. Li, Y. He, Y. Zhu, L. Jiang, S. Zhang, J. Qin, Q. Wu, W. Dai, S. Shen, Z. Pang, J. Wang, Route to rheumatoid arthritis by macrophage-derived microvesicle-coated nanoparticles, Nano Lett. 19 (1) (2019) 124–134.

[36] D.D. Brand, K.A. Latham, E.F. Rosloniec, Collagen-induced arthritis, Nat. Protoc. 2 (5) (2007) 1269–1275.

[37] J.J. Inglis, E. Simelyte, F.E. McCann, G. Criado, R.O. Williams, Protocol for the induction of arthritis in C57BL/6 mice, Nat. Protoc. 3 (4) (2008) 612–618.

[38] F. Chen, Y. Xing, Z. Wang, X. Zheng, J. Zhang, K. Cai, Nanoscale polydopamine (PDA) meets pi-pi interactions: an interface-directed coassembly approach for mesoporous nanoparticles, Langmuir 32 (46) (2016) 12119–12128.

[39] Q. Zheng, H. Shen, Z. Tong, L. Cheng, Y. Xu, Z. Feng, S. Liao, X. Hu, Z. Pan, Z. Mao, Y. Wang, A thermosensitive, reactive oxygen species-responsive, MR409-encapsulated hydrogel ameliorates disc degeneration in rats by inhibiting the secretory autophagy pathway, Theranostics 11 (1) (2021) 147–163.

[40] S. Hayer, M.J. Vervoordeldonk, M.C. Denis, M. Armaka, M. Hoffmann, J. Backlund, K.S. Nandakumar, B. Niederreiter, C. Geka, A. Fischer, N. Woodworth, S. Bluml, G. Kollias, R. Holmdahl, F. Apparailly, M.I. Koenders, 'SMASH' recommendations for standardised microscopic arthritis scoring of histological sections from inflammatory arthritis animal models, Ann. Rheum. Dis. (2021).

[41] C.M. Weyand, J.J. Goronzy, The immunology of rheumatoid arthritis, Nat. Immunol. 22 (1) (2021) 10–18.

[42] A.I. Catrina, C.I. Svensson, V. Malmstrom, G. Schett, L. Klareskog, Mechanisms leading from systemic autoimmunity to joint-specific disease in rheumatoid arthritis, Nat. Rev. Rheumatol. 13 (2) (2017) 79–86.

[43] 2nd, A. Accelerating Medicines Partnership Rheumatoid, C. Systemic Lupus Erythematosus F. Zhang, K. Wei, K. Slowikowski, C.Y. Fonseka, D.A. Rao, S. Kelly, S.M. Goodman, D. Tabechian, L.B. Hughes, K. Salomon-Escoto, G.F.M. Watts, A. H. Jonsson, J. Rangel-Moreno, N. Meednu, C. Rozo, W. Apruzzese, T. M. Eisenhaure, D.J. Lieb, D.L. Boyle, A.M. Mandelin, B.F. Boyce, E. DiCarlo, E. M. Gravallese, P.K. Gregersen, L. Moreland, G.S. Firestein, N. Hacohen, C. Nusbaum, J.A. Lederer, H. Perlman, C. Pitzalis, A. Filer, V.M. Holers, V. P. Bykerk, L.T. Donlin, J.H. Anolik, M.B. Brenner, S. Raychaudhuri, Defining inflammatory cell states in rheumatoid arthritis joint synovial tissues by integrating single-cell transcriptomics and mass cytometry, Nat. Immunol. 20 (7) (2019) 928–942.

[44] C.D. Buckley, C. Ospelt, S. Gay, K.S. Midwood, Location, location, location: how the tissue microenvironment affects inflammation in RA, Nat. Rev. Rheumatol. 17 (4) (2021) 195–212.

[45] C.M. Hedrich, G.C. Tsokos, Bridging the gap between autoinflammation and autoimmunity, Clin. Immunol. 147 (3) (2013) 151–154.

[46] Z. Szekanecz, I.B. McInnes, G. Schett, S. Szamosi, S. Benko, G. Szucs, Autoinflammation and autoimmunity across rheumatic and musculoskeletal diseases, Nat. Rev. Rheumatol. 17 (10) (2021) 585–595.

[47] A. Ablasser, S. Hur, Regulation of cGAS- and RLR-mediated immunity to nucleic acids, Nat. Immunol. 21 (1) (2020) 17–29.

[48] J. Ahn, D. Gutman, S. Saijo, G.N. Barber, STING manifests self DNA-dependent inflammatory disease, Proc. Natl. Acad. Sci. U. S. A. 109 (47) (2012) 19386–19391.

[49] L. Yu, P. Liu, Cytosolic DNA sensing by cGAS: regulation, function, and human diseases, Signal Transduct. Targeted Ther. 6 (1) (2021) 170.

[50] J. Willemsen, M.T. Neuhoff, T. Hoyler, E. Noir, C. Tessier, S. Sarret, T.N. Thorsen, A. Littlewood-Evans, J. Zhang, M. Hasan, J.S. Rush, D. Guerini, R.M. Siegel, TNF leads to mtDNA release and cGAS/STING-dependent interferon responses that support inflammatory arthritis, Cell Rep. 37 (6) (2021), 109977.

[51] R. Kreienkamp, S. Graziano, N. Coll-Bonfill, G. Bedia-Diaz, E. Cybulla, A. Vindigni, D. Dorsett, N. Kubben, L.F.Z. Batista, S. Gonzalo, A cell-intrinsic interferon-like response links replication stress to cellular aging caused by progerin, Cell Rep. 22 (8) (2018) 2006–2015.

[52] H. Ma, W. Qian, M. Bambouskova, P.L. Collins, S.I. Porter, A.K. Byrum, R. Zhang, M. Artyomov, E.M. Oltz, N. Mosammaparast, J.J. Miner, M.S. Diamond, Barrier-to-Autointegration factor 1 protects against a basal cGAS-STING response, mBio 11 (2) (2020).

[53] C.A. Juan, J.M. Perez de la Lastra, F.J. Plou, E. Perez-Lebena, The chemistry of reactive oxygen species (ROS) revisited: outlining their role in biological macromolecules (DNA, lipids and proteins) and induced pathologies, Int. J. Mol. Sci. 22 (9) (2021).

[54] S. Li, Z. Hong, Z. Wang, F. Li, J. Mei, L. Huang, X. Lou, S. Zhao, L. Song, W. Chen, Q. Wang, H. Liu, Y. Cai, H. Yu, H. Xu, G. Zeng, Q. Wang, J. Zhu, X. Liu, N. Tan, C. Wang, The cyclopeptide astin C specifically inhibits the innate immune CDN sensor STING, Cell Rep. 25 (12) (2018) 3405–3421, e7.

[55] Q. Zhao, Y. Wei, S.J. Pandol, L. Li, A. Habtezion, STING signaling promotes inflammation in experimental acute pancreatitis, Gastroenterology 154 (6) (2018) 1822–1835, e2.

[56] S. Benmerzoug, S. Rose, B. Bounab, D. Gosset, L. Duneau, P. Chenuet, L. Mollet, M. Le Bert, C. Lambers, S. Geleff, M. Roth, L. Fauconnier, D. Sedda, C. Carvalho, O. Perche, D. Laurenceau, B. Ryffel, L. Apetoh, A. Kiziltunc, H. Uslu, F.S. Albez, M. Akgun, D. Togbe, V.F.J. Quesniaux, STING-dependent sensing of self-DNA drives silica-induced lung inflammation, Nat. Commun. 9 (1) (2018) 5226.
[57] K.R. King, A.D. Aguirre, Y.X. Ye, Y. Sun, J.D. Roh, R.P. Ng Jr., R.H. Kohler, S. P. Arlauckas, Y. Iwamoto, A. Savol, R.I. Sadreyev, M. Kelly, T.P. Fitzgibbons, K. A. Fitzgerald, T. Mitchison, P. Libby, M. Nahrendorf, R. Weissleder, IRF3 and type I interferons fuel a fatal response to myocardial infarction, Nat. Med. 23 (12) (2017) 1481–1487.
[58] K. Mukai, H. Konno, T. Akiba, T. Uemura, S. Waguri, T. Kobayashi, G.N. Barber, H. Arai, T. Taguchi, Activation of STING requires palmitoylation at the Golgi, Nat. Commun. 7 (2016), 11932.
[59] Y. Xing, J. Zhang, F. Chen, J. Liu, K. Cai, Mesoporous polydopamine nanoparticles with co-delivery function for overcoming multidrug resistance via synergistic chemo-photothermal therapy, Nanoscale 9 (25) (2017) 8781–8790.
[60] Z. Yuan, C. Lin, L. Dai, Y. He, J. Hu, K. Xu, B. Tao, P. Liu, K. Cai, Near-infrared light-activatable dual-action nanoparticle combats the established biofilms of methicillin-resistant Staphylococcus aureus and its accompanying inflammation, Small 17 (13) (2021), e2007522.
[61] P. Yang, F. Zhu, Z. Zhang, Y. Cheng, Z. Wang, Y. Li, Stimuli-responsive polydopamine-based smart materials, Chem. Soc. Rev. 50 (14) (2021) 8319–8343.
[62] Q. Guan, R. Guo, S. Huang, F. Zhang, J. Liu, Z. Wang, X. Yang, X. Shuai, Z. Cao, Mesoporous polydopamine carrying sorafenib and SPIO nanoparticles for MRI-guided ferroptosis cancer therapy, J. Contr. Release 320 (2020) 392–403.
[63] Z. Wang, Y. Zou, Y. Li, Y. Cheng, Metal-containing polydopamine nanomaterials: catalysis, energy, and theranostics, Small 16 (18) (2020), e1907042.
[64] S. Tardito, G. Martinelli, S. Soldano, S. Paolino, G. Pacini, M. Patane, E. Alessandri, V. Smith, M. Cutolo, Macrophage M1/M2 polarization and rheumatoid arthritis: a systematic review, Autoimmun. Rev. (2019), 102397.
[65] J.S. Smolen, D. Aletaha, A. Barton, G.R. Burmester, P. Emery, G.S. Firestein, A. Kavanaugh, I.B. McInnes, D.H. Solomon, V. Strand, K. Yamamoto, Rheumatoid arthritis, Nat. Rev. Dis. Prim. 4 (2018), 18001.
[66] Q. Chen, L. Sun, Z.J. Chen, Regulation and function of the cGAS-STING pathway of cytosolic DNA sensing, Nat. Immunol. 17 (10) (2016) 1142–1149.
[67] K.N. Miller, S.G. Victorelli, H. Salmonowicz, N. Dasgupta, T. Liu, J.F. Passos, P. D. Adams, Cytoplasmic DNA: sources, sensing, and role in aging and disease, Cell 184 (22) (2021) 5506–5526.
[68] G.N. Barber, Innate immune DNA sensing pathways: STING, AIMII and the regulation of interferon production and inflammatory responses, Curr. Opin. Immunol. 23 (1) (2011) 10–20.